

TR AE 6504

A COMPARATIVE STUDY OF STEADY AND  
NONSTEADY-FLOW ENERGY SEPARATORS

by

Joseph S. Hashem

CONTRACT NO. DA-31-124-ARO-D-318  
U. S. Army Research Office-Durham

A Thesis Submitted to the Faculty of the Department of  
Aeronautical Engineering and Astronautics in Partial Fulfillment  
of the Requirements for the Degree of Master of Aeronautical  
Engineering.

RENSSELAER POLYTECHNIC INSTITUTE  
TROY, NEW YORK

OCTOBER 1965

*Ad 624 147*

*20050228012*

Best Available Copy

# TABLE OF CONTENTS

	Page
LIST OF SYMBOLS.....	iv
ABSTRACT.....	vi
INTRODUCTION AND HISTORICAL REVIEW.....	1
PART I. THE RANQUE-HILSCH TUBE.....	4
I-A. Flow in the Free Vortex.....	4
I-B. Flow in the Forced Vortex.....	6
1. Relationship between $\omega$ and $k$ .....	8
2. Determination of the temperature near the wall ( $T_w$ ).....	9
3. Numerical Solution.....	9
I-C. Comparison with Experimental Results.....	12
PART II. THE NON-STEADY FLOW ENERGY SEPARATOR.....	14
II-A. General Equations.....	14
II-B. Comparison with Vortex Tube.....	16
PART III. COEFFICIENT OF PERFORMANCE.....	19
III-A. Conventional Gas Refrigerating Machine.....	19
III-B. Energy Separators.....	19
III-C. Comparison of Energy Separators with Standard Refrigerating Machines.....	20
DISCUSSION OF RESULTS AND CONCLUSIONS.....	22
REFERENCES AND BIBLIOGRAPHY.....	24

# LIST OF SYMBOLS

$$A = T_w - B r^2$$

$$B = \omega^2 / 2 c_p g$$

$C$  flow velocity relative to frame  $F_s$  in which the flow field is stationary

$C_p$  specific heat at constant pressure

$e, e_1, e_2$  constants

$g$  gravitational acceleration

$H^o$  total stagnation enthalpy of a mass occupying a unit length of tube at station  $r$  (see Fig. I-1a)

$h, h^o$  static, stagnation enthalpy per unit mass

$k$  constant

$M$  total angular momentum of a mass occupying a unit length of tube at station  $r$  (see Fig. I-1a)

$m$  mass of gas which occupies a unit of length of the vortex tube at station  $r$

$\dot{m}$  mass flow rate

$$P_j = \left[ 1 - \frac{B r^2}{T_w} \left( 1 - \frac{r^2}{R^2} \right) \right]^{r/r-1}$$

$p, p^o$  static, stagnation pressure, respectively

$R$  rotor radius

$R$  gas constant

$r$  radial distance from vortex-tube axis

$S$  cross sectional area of vortex tube

$T, T^o$  static, stagnation temperature, respectively

$$u_o^2 = 2 h_i^o \left[ 1 - \left( p_2/p_i^o \right)^{r-1/r} \right]$$

$u$  flow velocity relative to frame of reference  $F_u$ , in which energy separation is utilized

$u_v$  whirl in frame  $F_u$

$V$  rotor peripheral speed

$V_{i1}$	injection velocity
$v$	tangential velocity of flow at station (1)
$\alpha$	inclination of the flow to plane of rotation at runner inlet
$\theta$	see Fig. II-1a, II-1b and II-2b
$\gamma$	ratio of specific heats
$\mu = \dot{m}_b / \dot{m}_a$	
$\omega$	angular velocity of fluid in the forced vortex
$\rho$	fluid density

#### Subscripts

a,b	cold, hot stream, respectively
d	discharge
i	irrotational
r	rotational
w	wall
1 through 5	See Fig. II-2a

## ABSTRACT

This paper analyzes and compares two methods of energy separation -- a steady-flow method proposed by Ranque over thirty years ago and a nonsteady-flow method recently proposed and studied by Foa.

Part I of this paper develops a simple theory for devices utilizing the first method (Ranque tubes). Despite its simplicity and extreme idealization, the theory appears to provide better agreement with experimental data than any of the available analytical treatments.

Part II is an extension of the Foa theory of the non-steady-flow energy separator. The extension is more idealized than the original theory but covers a wider variety of embodiments of the concept. A comparison is also given between the performance characteristics of steady-flow and non-steady-flow energy separators.

Part III defines a coefficient of performance for the two devices as refrigerators or air conditioners, and compares these coefficients with those of standard refrigerating cycles.

## INTRODUCTION AND HISTORICAL REVIEW

What is known today as the Ranque-Hilsch effect was first discovered in 1931 by George Joseph Ranque, a French metallurgist associated with a steel company in the town of Montlouçon, Central France. It is not known how Ranque made this discovery, but it is assumed that he noticed such an effect in connection with cyclone separators, where the air drawn from the center is slightly cooler than the air drawn from the periphery. He sought to utilize this effect in the device which is now known as the vortex tube, Ranque tube, or improperly, the Hilsch tube. For this device he obtained a French patent in 1932 and a United States patent (No. 1,952,281) in 1934.

The vortex tube is extremely simple and has no moving parts. It consists of a straight tube provided with an orifice which allows a supply of compressed gas to be injected tangentially into the tube. This stream of compressed gas divides into two streams at different temperatures -- the cold stream leaving through the center and the hot stream through the periphery.

Ranque was obviously hoping to accomplish significant changes in refrigeration with his invention, but subsequent development showed this device to be very inefficient as a refrigerator. Nothing more was heard about it until 1945, when it was learned that during the war the vortex tube had been studied in Germany by Rudolph Hilsch, a physicist of the University of Erlangen. Publication of a paper by Hilsch (Ref. 1) aroused much interest in the device in the United States.

Since 1946, several attempts have been made to explain the curious phenomenon taking place inside this tube. It is now understood that when a

stream of compressed gas is injected tangentially into a tube of constant cross section, a free vortex is formed due to the absence of any external torque. The velocity profile in this vortex is that of an irrotational flow, with constant angular momentum. The total energy of each particle in the free vortex is also constant. Therefore there is a continuous drop in temperature from the walls of the tube to the axis. A free vortex cannot, however, be maintained in a real gas, due to the presence of viscosity.

Therefore, the flow cannot maintain a constant energy distribution as it proceeds down the tube. The fast moving inner layers lose part of their kinetic energy to the outer layers and are slowed down. The conversion from irrotational to rotational flow is completed near the discharge end, where the vortex becomes completely forced ( $\omega = \text{constant}$ ).

In the forced vortex the flow is highly turbulent and the changes in state properties associated with the convection of small masses of fluid in this turbulent flow obey the isentropic law  $p/\rho^\gamma = \text{constant}$ . Therefore both the kinetic energy and the static temperature distribution which complies with this law are higher at the walls of the tube than in the center. If, then, the flow is divided into two separate, concentric flows along any desired radius, two streams at different stagnation temperatures are obtained.

Kassner and Knoernschild (Ref. 2) contributed much to the understanding of this phenomenon, through analyses in which they calculated temperature and velocity profiles in rotational and irrotational flows of fluids of constant density.

Part I of the present paper gives a simplified analytical study of a compressible flow in a uniflow\* vortex tube. In this theory the variation

---

\* In the uniflow type tube the cold and hot streams leave the vortex tube through the same end, whereas in the counterflow vortex tube the two streams leave through opposite ends. See Fig. I-1a.

in density, which was left out in the Kassner-Knoernschild analysis, is taken into account. The results obtained from this theory agree very well with Hilsch's experimental results given in Ref. 1.

Also treated on a more general basis, in Part II, is an energy separator proposed by Foa (Ref. 3), which represents the unsteady-flow counterpart of the vortex tube. In this device, the process by which the original homogeneous stream of compressed gas separates into two streams at different temperatures is an essentially nondissipative "crypto-steady" process. A crypto-steady process is one which is nonsteady in the frame of reference  $F_u$  in which it is observed and utilized but admits a frame of reference  $F_s$  in which it is steady. This process is easily analyzed as a steady-flow process in this unique frame of reference, while retaining the advantages of nonsteady flow processes in the frame of reference in which it is used.

The production of cold and hot streams in the nonsteady-flow energy separator can be explained briefly by reference to Fig. II-1a. Here (i) represents the initial homogeneous jet, which divides into streams a and b upon impinging on a wall. The surface of contact (s) between the two flows a and b in the original stream is stationary in frame  $F_s$ , but is moving in any other frame of reference  $F_u$ . The pressure forces acting on this surface are therefore doing work in  $F_u$ . The work done by these pressure forces is equal to the energy transferred from the one flow to the other.

Part III of this paper is devoted to the definition and calculation of suitable coefficients of performance for both the vortex tube and the nonsteady-flow energy separator, and to the comparison of these with the coefficient of performance of a standard refrigerating cycle (reversed Brayton cycle).



# PART I

## THE RANQUE-HILSCH TUBE

### I-A. Flow in the Free Vortex

Immediately after injection the flow is irrotational and free from external torque. Therefore, at this injection end

$$vr = k \quad (1)$$

where  $k$  is a constant.

For radial equilibrium,

$$\frac{1}{\rho} \frac{\partial p}{\partial r} = \frac{v^2}{r} \quad (2)$$

Therefore, at the injection station

$$dp = \rho \frac{k^2}{r^3} dr \quad (3)$$

Since the stagnation enthalpy is uniform at station (i), neglecting the axial component of the flow velocity at that station one has

$$\begin{aligned} c_p T_i^0 &= c_p T_i + \frac{k^2}{2gr^2} \\ T_i &= T_i^0 - \frac{k^2}{2c_p gr^2} \end{aligned} \quad (4)$$

Combining equation (i) with the equation of state for a perfect gas and utilizing (3) one obtains

$$\frac{dp}{p} = \frac{\gamma}{\gamma-1} \frac{k^2 dr}{r(2c_p g T_i^0 r^2 - k^2)}$$

which when integrated yields

$$\ln \frac{p_i}{p_{iw}} = \frac{\gamma}{\gamma-1} \ln \frac{2gc_p T_i^0 - k^2/r^2}{2gc_p T_i^0 - k^2/r_w^2}$$

or

$$P_i = P_{i\infty} \left[ \frac{2 C_p g T_i^{\circ} - k^2/r^2}{2 C_p g T_{i\infty}^{\circ} - k^2/r_{\infty}^2} \right]^{1/\gamma-1} \quad (5)$$

Equation (5) gives the pressure distribution in the free vortex.

The density distribution is easily obtained from equation (4) and the equation of state, which give

$$\rho_i = \frac{1}{gR} \frac{P_{i\infty}}{(T_i^{\circ} - k^2/2 C_p g r^2)} \left[ \frac{2 g C_p T_i^{\circ} - k^2/r^2}{2 g C_p T_{i\infty}^{\circ} - k^2/r_{\infty}^2} \right]^{1/\gamma-1}$$

or

$$\rho_i = 2 C_p g T_{i\infty} \rho_{i\infty} \frac{(2 C_p g T_i^{\circ} - k^2/r^2)^{1/\gamma-1}}{(2 C_p g T_{i\infty}^{\circ} - k^2/r_{\infty}^2)^{1/\gamma-1}} \quad (6)$$

By virtue of the conservation of angular momentum, the expression for the total angular momentum integrated over the mass  $m$  which occupies a unit length of tube at station  $r$  is given by

$$M_i = m k$$

Similarly, because of the uniformity of the total energy distribution the integrated stagnation enthalpy can be written in the form

$$H_i^{\circ} = m C_p T_i^{\circ}$$

The velocity, according to the distribution given by equation (1) and shown in Figure I-2 would increase indefinitely as the radius tends to zero. The fluid is however taken to be irrotational down to a nucleus radius  $r_1$ , which is arbitrarily specified to be that at which the temperature of the gas would reach absolute zero. Furthermore it is assumed that the region lying inside  $r_1$ , and extending through the whole length of the tube, is replaced by a solid core of the same dimensions.

The expression for  $r_1$  is easily obtained by letting  $T_1$  equal zero in equation (4). Thus,

$$r_1^2 = \frac{k^2}{2 C_p g T_c} \quad (9)$$

#### I-B. Flow in the Forced Vortex

The flow in the forced vortex will now be studied on the basis of the following simplifying assumptions:

- (a) there is no exchange of energy between the flow inside the tube and the surroundings.
- (b) the friction at the walls is negligible, and
- (c) at the discharge end, the axial velocity is uniform and the radial velocity zero.

As mentioned previously, the pressure and temperature distributions at the discharge end obey the isentropic law

$$p/\rho^{\gamma} = \text{constant} \quad (10)$$

This, combined with the equation of state and the expression for the centrifugal pressure gradient, gives the distribution of temperature along the radius in terms of the two unknown parameters  $T_w$  and  $\omega$ .

To determine these two quantities, use will be made of the fact that the total angular momentum, the total energy, and the total mass crossing this section in unit of time are the same as at the injection section (where free vortex flow prevails).

Following the same procedure as before, the expression for radial equilibrium becomes

$$dp = \rho \omega^2 r dr \quad (11)$$

Using the equation of state, equation (10) can be rewritten as

$$p = e_2 T^{r/r-1} \quad (12)$$

or

$$p = e_3 T^{1/r-1}$$

Combining equations (10) and (12) one obtains

$$dT = \frac{r-1}{r} \frac{e_3}{e_2} \omega^2 r dr$$

which, when integrated, yields the desired expression for the variation of the temperature along the radius.

$$T_r = T_w + \frac{\omega^2 r_w^2}{2c_p g} \left( \frac{r^2}{r_w^2} - 1 \right) \quad (13)$$

On the other hand, by definition

$$T_r^o = T_r + \frac{\omega^2 r^2}{2c_p g}$$

Therefore,

$$T_r^o = T_w + \frac{\omega^2 r^2}{2c_p g} \left( \frac{2r^2}{r_w^2} - 1 \right) \quad (14)$$

The expressions for the density and pressure are readily obtained from equations (12) and (13), thus giving

$$p_r = e_2 \left[ T_w + \frac{\omega^2 r_w^2}{2c_p g} \left( \frac{r^2}{r_w^2} - 1 \right) \right]^{1/r-1} \quad (15)$$

or

$$p_r = p_w \left[ 1 + \frac{\omega^2 r_w^2}{2c_p g T_w} \left( \frac{r^2}{r_w^2} - 1 \right) \right]^{1/r-1} \quad (16)$$

and

$$p_r = p_w \left[ 1 + \frac{\omega^2 r_w^2}{2c_p g T_w} \left( \frac{r^2}{r_w^2} - 1 \right) \right]^{r/r-1} \quad (17)$$

Remembering that  $m$  is the mass of gas in a unit length of

the tube at the rotational end:

$$m = 2\pi \int_{r_1}^{r_2} \rho r dr$$

Substituting for  $\rho$  from equation (15) and integrating, one obtains

$$m = \frac{\pi e_3}{r_2^{r/r-1}} \left[ (A + Br_2^2)^{r/r-1} - (A + Br_1^2)^{r/r-1} \right] \quad (18)$$

or

$$(A + Br_1^2)^{r/r-1} = T_w^{r/r-1} - \frac{\frac{r}{r-1} m B}{\pi e_3} \quad (19)$$

where

$$A = T_w - Br_w^2$$

$$B = \omega^2 / 2r_p g$$

#### 1. Relation Between $\omega$ and $k$ .

For the rotational flow, the expression for the angular momentum is given by

$$M_r = 2\pi \int_{r_1}^{r_2} \rho \omega r^3 dr$$

which when integrated by parts gives

$$M_r = \frac{\pi \omega e_3}{\frac{2r-1}{r-1} B} \left[ r_2^2 (A + Br_2^2)^{r/r-1} - r_1^2 (A + Br_1^2)^{r/r-1} - \frac{Am}{\pi e_3} \right] \quad (20)$$

Equations (18), (19), and (20) give

$$M_r = \frac{\pi \omega e_3}{\frac{2r-1}{r-1} B} \left[ T_w^{r/r-1} (r_2^2 - r_1^2) \right] + \frac{r}{2r-1} m \omega r_1^2 - \frac{A \omega m}{\frac{2r-1}{r-1} B}$$

Equating the total angular momenta  $M_i$  and  $M_r$ , one finally obtains

$$k = \frac{r}{2\gamma-1} \omega r^2 \left(1 - \frac{r_i^2}{r^2}\right) \left[ \frac{1}{1 - \left[1 - \frac{\theta r_i^2}{T_c} \left(1 - r_i^2/r^2\right)\right]^{1/\gamma-1}} \right] + \frac{r \omega r_i^2}{2\gamma-1} - \frac{A \omega}{\frac{2\gamma-1}{\gamma-1} B} \quad (21)$$

## 2. Determination of the Temperature at the Wall ( $T_w$ )

The total stagnation enthalpy per unit length of the tube in the rotational flow is

$$\begin{aligned} h_r &= 2\pi \int_{r_i}^{r_w} c_p T_r^\circ \rho_r r dr \\ \text{or} \quad H_r^\circ &= \pi \int_{r_i}^{r_w} c_p T_r^\circ \rho_r dr^2 + \pi \int_{r_i}^{r_w} \rho_r \frac{\omega^2 r^2}{2g} dr^2 \\ &= \pi c_p e_3 \int_{r_i}^{r_w} (A + B r^2)^{1/\gamma-1} dr^2 + \frac{\omega}{2g} M_r \end{aligned}$$

Substituting  $mk$  for  $M_r$  in the above expression and integrating one obtains

$$H_r^\circ = \frac{\pi c_p e_3}{\frac{2\gamma-1}{\gamma-1} B} \left[ \frac{\frac{2\gamma-1}{\gamma-1} B mk}{\pi \omega e_3} + \frac{m A}{\pi e_3} + \frac{\frac{r}{\gamma-1} m A}{\pi e_3} \right] + \frac{\omega m k}{2g}$$

Equating the total stagnation enthalpies  $H_i^\circ$  and  $H_r^\circ$  and making use of equation (18) and (20), one obtains

$$\begin{aligned} T_c^\circ &= A + \frac{\omega k}{c_p g} \\ \text{or} \quad T_w &= T_c^\circ + \frac{\omega^2 r_w^2}{2c_p g} - \frac{\omega k}{c_p g} \end{aligned} \quad (22)$$

## 3. Numerical Solution

Equation (21) cannot be solved explicitly for  $\omega$ . It becomes therefore necessary at this point to determine the temperature distribution numerically for each specific case.

Given  $k$ , the corresponding values of  $\omega$  and  $T_w$  can be determined as follows:

Assigning first the value zero to the quantity  $P_j = \left[ 1 - \frac{8C^2}{T_w} \left( 1 - \frac{r_1^2}{r_w^2} \right) \right]^{1/2}$  in equation (21), the corresponding values of  $\omega_j$  and  $T_{wj}$  can be obtained. The quantity  $P_{j+1}$  is calculated using these values. By substitution back in equation (21), new values  $\omega_{j+1}$  and  $T_{wj+1}$  are obtained. The process is continued till successive values of  $P_{j+n}$  become sufficiently close to one another.

Two cases are analyzed here, pertaining to injection velocities ( $V_{i1} = k/r_w$ ) of 1000 and 750 fps. Tables I-1 and I-2 list the results of such computations. The ratio  $r_1/r_w$  in equation (21) is determined in each case by equation (9).

TABLE I-1:  $V_1 = 1000$  f.p.s.,  $r_1/r_w = 0.4$ ,  $T_1^0 = 528^\circ\text{R}$  and  $\gamma = 1.4$ 

1st Iteration	2nd Iteration	3rd Iteration	4th Iteration
$P_j = 0$	$P_{j+1} = 0.132$	$P_{j+2} = 0.181$	$P_{j+3} = 0.203$
$wr_w = 1758$ f.p.s.	$wr_w = 1625$ f.p.s.	$wr_w = 1570$ f.p.s.	$wr_w = 1555$ f.p.s.
$T_w = 494^\circ\text{R}$	$T_w = 479^\circ\text{R}$	$T_w = 472^\circ\text{R}$	$T_w = 470^\circ\text{R}$
$P_{j+1} = 0.132$	$P_{j+2} = 0.181$	$P_{j+3} = 0.203$	$P_{j+4} = 0.209$

TABLE I-2:  $V_1 = 750$  f.p.s.,  $r_1/r_w = 0.3$ ,  $T_1^0 = 528^\circ\text{R}$  and  $\gamma = 1.4$ 

1st Iteration	2nd Iteration	3rd Iteration	4th Iteration
$P_j = 0$	$P_{j+1} = 0.194$	$P_{j+2} = 0.275$	$P_{j+3} = 0.316$
$wr_w = 1643$ f.p.s.	$wr_w = 1460$ f.p.s.	$wr_w = 1378$ f.p.s.	$wr_w = 1335$ f.p.s.
$T_w = 548^\circ\text{R}$	$T_w = 523^\circ\text{R}$	$T_w = 514^\circ\text{R}$	$T_w = 510^\circ\text{R}$
$P_{j+1} = 0.194$	$P_{j+2} = 0.275$	$P_{j+3} = 0.316$	$P_{j+4} = 0.341$
	5th Iteration	6th Iteration	
	$P_{j+4} = 0.341$	$P_{j+5} = 0.362$	
	$wr_w = 1295$ f.p.s.	$wr_w = 1290$ f.p.s.	
	$T_w = 506^\circ\text{R}$	$T_w = 505^\circ\text{R}$	
	$P_{j+5} = 0.362$	$P_{j+6} = 0.365$	



### I-C. Comparison with Experimental Results

Setting  $p_{r_{\min}} = p_d$

$$\frac{p_i^0}{p_d} = \frac{p_i^0}{p_w} \frac{p_w}{p_{r_{\min}}}$$

Furthermore, since the pressure at the wall remains substantially uniform throughout (Ref. 4, Part 1), the ratio  $p_i^0/p_d$  can be written as follows:

$$\frac{p_i^0}{p_d} = \frac{p_i^0}{p_w} \frac{p_w}{p_{r_{\min}}} \quad (23)$$

where

$$\left( \frac{p_i^0}{p_w} \right) = \left( \frac{T_i^0}{T_w} \right)^{r/r-1}$$

and  $p_{r_w}/p_{r_{\min}}$  is obtained from equation (17) with  $r = r_1$ . Equation (23) gives, for the two velocities of 1000 and 750 f.p.s. considered here, the pressure ratios of 8.15 and 3.78 respectively.

Figure I-3 shows the variation of the pressure along the radius in the irrotational flow. Figures I-4 and I-5 show the variation in density and pressure along the radius for the rotational case.

Now define

$$\begin{aligned} \mu &= \bar{m}_b / \bar{m}_a \\ &= \frac{\bar{\rho}_b (1 - r^2/r_w^2)}{\bar{\rho}_a \left( \frac{r^2 - r_w^2}{r_w^2} \right)} \end{aligned}$$

where barred quantities represent average densities given by

$$\bar{\rho} = \frac{\sum_j \rho_j s_j}{\sum_j s_j}$$

and computed using Figure I-4.

From equation (14), (22), (24) and using the data given in the last column of Tables I-1 and I-2, a final plot of  $T^0$  vs  $\frac{1}{1+\mu}$  can be made for the

two values of the parameter  $p_i^0/p_d$  of 8.15 and 3.78 and is shown in Figure I-6. Also plotted on the same graph for comparison are the experimental results obtained by Hilsch in Ref. 1 and the simplified theory due to Kassner and Knoernschild (Ref. 2). The agreement between the theory presented above and Hilsch's result is surprisingly good especially for large values of  $\frac{1}{1+\mu}$ , i.e., in the range where this device would be expected to be most useful as a refrigerator.

## PART II

### THE NONSTEADY FLOW ENERGY SEPARATOR

#### II-A. General Equations

The Foa concept of non-steady-flow energy separation lends itself to embodiment in a great variety of arrangements. Only the simplest of these (shown in Fig. II-1b) is analyzed in Ref. 3, for the purpose of illustration. The following treatment is an extension of Ref. 3. It is less exact, since it does not account for any dissipation or losses, but it is considerably more general, in that it covers most of the conceivable embodiments of the Foa concept.

In the simplest form of this separator, continuous flows exchange mechanical energy directly through the action of mutually exerted pressure forces at their interfaces. In more complex arrangements the energy transfer function is performed, in part or in full, by turbines and compressors, but the principle of operation is still the same, in that one portion of the initially homogeneous flow is made to do work on the remaining portion. The study of non-steady flow separation as a turbine-compressor action has the advantage of leading in a direct manner to the determination of the effects of the various controls that may be applied to the two flows.

The "generalized energy separator" considered here is diagrammatically shown in Fig. II-2a. There C denotes a compressor and  $t_1$  and  $t_2$  two impulse turbines which, together, drive the compressor. The two turbines are taken to be of the same diameter, and it is stipulated that  $t_2$  is so designed that the whirl at its exit is zero. Therefore, when  $t_2$  is present, the system is designed to produce the maximum extraction of power from flow a.

Thus,  $u_{v_{a_2}} = u_{a_2} \cos \alpha_{a_2} = 0$ . The assumption is now made that

$$u_{a_2} = u_{a_1} = u_0 \quad \text{and} \quad V_a = V_b = V$$

From inspection of Fig. II-2b, the following relations are obtained:

$$\begin{aligned}
 u_{va_2} &= u_o \cos \alpha_{a_2} \\
 c_{a_3}^2 &= c_{a_2}^2 = u_o^2 + V^2 - 2 V u_o \cos \alpha_{a_2} \\
 u_{a_3}^2 &= c_{a_3}^2 + V^2 + 2 V c_{a_3} \cos \theta_{a_3} \\
 u_{a_4} &= u_{a_3} \\
 u_{va_4} &= u_{a_3} \cos \alpha_{a_4} \\
 u_{va_5} &= c_{a_3} \cos \theta_{a_3} + V \\
 c_{a_5}^2 &= c_{a_4}^2 = u_{a_4}^2 + V^2 - 2 V u_{va_4} \\
 u_{a_5}^2 &= c_{a_5}^2 - V^2
 \end{aligned} \tag{1}$$

Similarly

$$\begin{aligned}
 u_{vb_2} &= u_o \cos \alpha_{b_2} \\
 c_{b_3}^2 &= c_{b_2}^2 = u_o^2 + V^2 - 2 V u_o \cos \alpha_{b_2} \\
 u_{b_3}^2 &= c_{b_3}^2 + V^2 + 2 V c_{b_3} \cos \theta_{b_3} \\
 u_{vb_3} &= c_{b_3} \cos \theta_{b_3} + V
 \end{aligned} \tag{2}$$

Therefore, one obtains

$$u_{a_3}^2 = u_o^2 + 2V^2 + 2V \left[ (u_o^2 + V^2 - 2Vu_o \cos \alpha_{a_2})^{1/2} \cos \theta_{a_3} - u_o \cos \alpha_{a_2} \right] \tag{3}$$

$$u_{a_5}^2 = u_{a_3}^2 - 2Vu_{a_3} \cos \alpha_{a_4} \tag{4}$$

and

$$u_{b_3}^2 = u_o^2 + 2V^2 + 2V \left[ (u_o^2 + V^2 - 2Vu_o \cos \alpha_{b_2})^{1/2} \cos \theta_{b_3} - u_o \cos \alpha_{b_2} \right] \tag{5}$$

The energy equation can be written in the following form

$$h_{a,1}^{\circ} + \mu h_{b,1}^{\circ} = (1 + \mu) h_i^{\circ} \quad (6)$$

and since the static enthalpy is the same at station 5 as at station 3

$$h_{b,5}^{\circ} - h_{a,5}^{\circ} = \frac{1}{2} (u_{b,5}^2 - u_{a,5}^2) \quad (7)$$

From equations (6) and (7) the following expressions can be deduced

$$\frac{h_i^{\circ} - h_{a,5}^{\circ}}{u_o^2} = \frac{\mu}{1 + \mu} \frac{(u_{b,5}^2 - u_{a,5}^2)}{2 u_o^2} \quad (8)$$

and

$$\frac{h_{b,5}^{\circ} - h_i^{\circ}}{u_o^2} = \frac{1}{1 + \mu} \frac{(u_{b,5}^2 - u_{a,5}^2)}{2 u_o^2} \quad (9)$$

By means of equations (3), (4) and (5),  $u_{b,5}^2$  and  $u_{a,5}^2$  can be expressed in terms of  $V$  and  $u_o$  only.  $V$  is obtained as a function of  $\mu$  by equating the power output of the turbines to the work required to drive the compressor.

$$\begin{aligned} \text{Power output of turbines} &= \dot{m}_a V (u_{v_{a,2}} - u_{v_{a,3}}) + \dot{m}_a V (u_{v_{a,4}} - u_{v_{a,5}}) \\ &= \dot{m}_a V (u_{v_{a,2}} - u_{v_{a,3}} + u_{v_{a,4}}) \end{aligned}$$

$$\text{Power required to drive the compressor} = \dot{m}_b V (u_{v_{b,5}} - u_{v_{b,2}})$$

Therefore

$$\mu = \frac{u_{v_{a,2}} - u_{v_{a,3}} + u_{v_{a,4}}}{u_{v_{b,5}} - u_{v_{b,2}}} \quad (10)$$

#### B. Comparison with Vortex Tube

Equations (8) and (9) were solved for each of the following four

cases:

Case 1.

This is the only case involving the use of a turbine  $t_2$ , for maximum power extraction from the cold flow. This turbine helps to drive the rotor, thereby increasing its rotational speed and the stagnation temperature of the hot flow.

Case 2.

Prerotation is imparted to the entire flow at the entrance to the runner passages. This can be done either by means of stator vanes or by injecting the gas tangentially inside the rotor, as is done in the Ranque tube.

Case 3.

Prerotation is imparted to the cold flow only, by means of stator vanes at the entrance of the cold flow to the runner passages.

Case 4.

This is the case treated in Ref. 3. It involves no prerotation, no turbine  $t_2$ , and no stator vanes.

In each case, the performance was calculated for different values of the angles  $\theta_{b_1}$ ,  $\alpha_{a_1}$ ,  $\alpha_{b_1}$  and  $\alpha_{a_4}$ . Table II-1 lists the different values given to these angles in each case. For simplicity, the angle  $\theta_{a_1}$  was stipulated to be equal to  $180^\circ - \theta_{b_1}$  in all cases.

The results are plotted in Figs. II-3 through II-26. The results of the analysis of Part I are also plotted, for comparison, on the same graphs, as dotted curves. The numbers next to these curves refer to the pressure ratio ( $p_1^0/p_d$ ) to which they correspond, whereas the numbers next to the solid curves refer to the particular case at hand.

	$\alpha_{a_1}$	$\alpha_{b_1}$	$\alpha_{a_4}$	$\theta_{b_1}$
Case 1	$90^\circ$	$90^\circ$	$\neq 90^\circ$	$180^\circ - \theta_{a_1}$
Case 2	$\neq 90^\circ$	$\alpha_{a_1}$	$90^\circ$	$180^\circ - \theta_{a_1}$
Case 3	$\neq 90^\circ$	$90^\circ$	$90^\circ$	$180^\circ - \theta_{a_1}$
Case 4	$90^\circ$	$90^\circ$	$90^\circ$	$180^\circ - \theta_{a_1}$

TABLE II-1

Looking at Figs. II-3 through II-26, it is noticed that the curves corresponding to Case 1, above, give the highest temperature difference. In fact, this difference increases indefinitely as  $\mu$  approaches zero. This, of course, is physically impossible. However, a closer look reveals that the prerotation in the flow ahead of turbine  $t_2$  cannot be completely eliminated by expansion through this turbine if the magnitude of the velocity  $C_{a_4}$  is less than  $V$ . Therefore,

$$(C_{a_4})_{\min} = (C_{a_5})_{\min} = V$$

From equation (1),

$$(u_{a_4})_{\min} = 2 V \cos \alpha_{a_4} \quad (11)$$

The corresponding value of  $\mu$  (i.e., the minimum value of  $\mu$  compatible with the stipulation of zero exit whirl in flow a) is calculated by means of equation (10), with the value of  $V$  determined through simultaneous solution of the second and third of equations (1), and equation (11).

Therefore, in Figs. II-3 through II-26, only the parts of the curves beyond  $\mu_{\min}$  are physically meaningful.

## PART III

## THE COEFFICIENT OF PERFORMANCE

III-A. Conventional Gas Refrigerating Machine

The coefficient of performance of the energy separators will be calculated and compared with the coefficient of performance of a standard gas refrigerating machine, using a conventional compressor-turbine arrangement. The cycle normally used in such machines is the reversed Brayton cycle, (see Ref. 5) where -- ideally -- the gas is compressed isentropically in a compressor from a state  $a'$  to a state  $b'$  (see Figure III-1a), cooled at constant pressure from  $b'$  to  $c'$ , then expanded through a turbine from  $c'$  to  $d'$  (where the pressure is the same as at  $a'$ ), while doing work. This work is utilized to help drive the compressor. The cold gas is then discharged producing a continuous flow of cold gas.

The coefficient of performance for such a device may be defined as the heat removed from the cold flow divided by the work of isentropic compression. Therefore

$$\text{C.P.} = \frac{(h_{c'} - h_{d'})}{(h_{b'} - h_{a'}) - (h_{c'} - h_{d'})}$$

Since  $p_{a'}/p_{b'} = p_{d'}/p_{c'}$ , the expression for C.P. reduces to

$$\text{C.P.} = \frac{1}{\left[ (p_{c'}/p_{d'})^{1/\gamma} - 1 \right]} \quad (1)$$

III-B. Energy Separators

In the case of the energy separators, the gas is first compressed



isentropically through a compressor, then cooled at constant pressure in a heat exchanger before being allowed to separate into cold and hot streams. Therefore, using the same definition as before, the expression for the coefficient of performance of steady and nonsteady-flow energy separators becomes:

$$C.P. = \frac{\dot{m}_a (h_i^o - h_a^o)}{(\dot{m}_a + \dot{m}_b)(h_i^o - h_d)}$$

If the energy of the hot stream can be regained, then

$$\begin{aligned} C.P. &= \frac{h_i^o - h_a^o}{(1+\mu)(h_i^o - h_d) - \mu(h_b^o - h_d)} \\ &= \frac{T_i^o - T_a^o}{T_i^o \left[ 1 - \left( \frac{p_d}{p_i^o} \right)^{\frac{\gamma-1}{\gamma}} \right] - \mu(T_b^o - T_i^o)} \quad (2) \end{aligned}$$

### III-C. Comparison of Energy Separators With Standard Refrigerating Machines

The coefficient of performance of a standard refrigerating machine operating in a closed cycle is independent of  $\mu$ , whereas that of the energy separators is not, as can be seen from equation (2). The quantity  $(T_i^o - T_a^o)$  and therefore the coefficient of performance, vary with  $\mu$ . By inspection of Figs. II-3 through II-26 it becomes evident that this quantity is largest for small values of  $\mu$ , high values of the ratio  $p_i^o/p_d$  and for the smallest possible angles  $\theta_{b_3}$ ,  $\alpha_{a_2}$ ,  $\alpha_{b_2}$  and  $\alpha_{a_4}$ .

Fig. III-1b compares the coefficient of performance of the non-steady-flow energy separator (Case 2, with  $\theta_{b_3} = 15^\circ$  and  $\alpha_{a_2} = \alpha_{b_2} = 30^\circ$ ),

with those of the vortex tube and of the standard refrigerating machine.

The coefficient of performance of the nonsteady flow energy separator is far superior to that of the vortex tube although still lower than that of the standard refrigerating machine. This difference, however, decreases as the pressure ratio  $p_1^0/p_d$  is increased.

## DISCUSSION OF RESULTS AND CONCLUSIONS

The results of the steady-flow energy separator theory (Part I of this paper) are summarized in Fig. I-6, which shows how well the new theory developed here agrees with the experimental results obtained by Hilsch over the whole range of mass flow ratios. The agreement is best for the smaller mass flow ratios, which are the ones of greatest interest when the device is used as a refrigerator. The simplified theory of Kassner and Knoernschild agrees very well with the experimental data for small mass flow ratios but not at all for the larger ratios.

The results of the nonsteady-flow energy separator theory, presented in Figs. II-3 through II-26, point to the possibility of substantial performance improvements over the statorless device which is analyzed as an illustrative example in Ref. 3. The statorless device, identified here as case 4, operates only for  $\mu < 1$ . Some of the modifications covered by the extended theory developed in Part II -- more specifically, those identified as cases 1, 2, and 3 -- produce better performance and are capable of operating over wider ranges of the mass flow ratio. In general, the performance can be improved by increasing the pressure ratio  $p_1^0/p_d$  and also by making the angles  $\theta_{b_1}$ ,  $\alpha_{a_2}$ ,  $\alpha_{b_1}$  and  $\alpha_{a_4}$  as small as possible.

The coefficient of performance of the nonsteady-flow energy separator is shown to be much higher than that of the vortex tube. The former is comparable to that of the standard refrigerating machine, and may even exceed it over a certain range of  $\mu$  and for pressure ratios  $p_1^0/p_d$  above 10, as can be seen from Fig. III-1b.

In summary the mechanism by which cold and hot streams are obtained in the Ranque tube is a highly dissipative one, and the only advantage of

this device as a refrigerator is in its extreme simplicity.

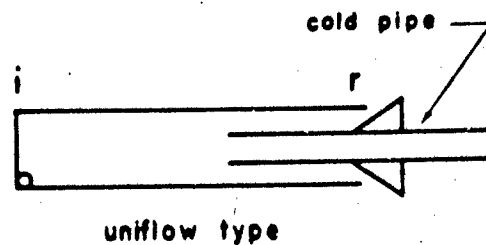
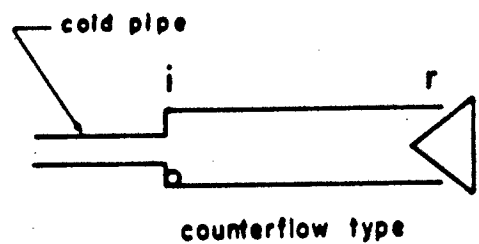
The performance of the non-steady flow energy separator is much better than that of the Ranque tube, due to the fact that essentially non-dissipative processes are responsible for the separation of energy. The theoretical coefficient of performance of this device is comparable to that of a standard refrigerating machine for low values of  $\mu$  and for high values of the ratio  $p_i^0/p_d$ .

## REFERENCES

1. Hilsch, R., "The Use of the Expansion of a Gas in a Centrifugal Field as a Cooling Process," Review of Scientific Instruments, Vol. 18, No. 2, February 1947, pp. 108 (unabridged translation).
  2. Knoernschild, E., Kassner, R., "Friction Laws and Energy Transfer in Circular Flow," Technical Report N-FTR-2198-ND. GS-USAF, Wright Patterson Air Force Base N-78, March 1948.
  3. Foa, J.V., "Energy Separator," Rensselaer Polytechnic Institute, Technical Report, TR AE 6401, January 1964.
  4. Lay, J.E., "An Experimental and Analytical Study of Vortex-Flow-Temperature Separation by Superposition of Spiral and Axial Flows," Journal of Heat Transfer, August 1959.
- 
5. Sears, F.W., Lee, J.F., "Thermodynamics," Addison-Wesley Publishing Co., Inc., 1955.

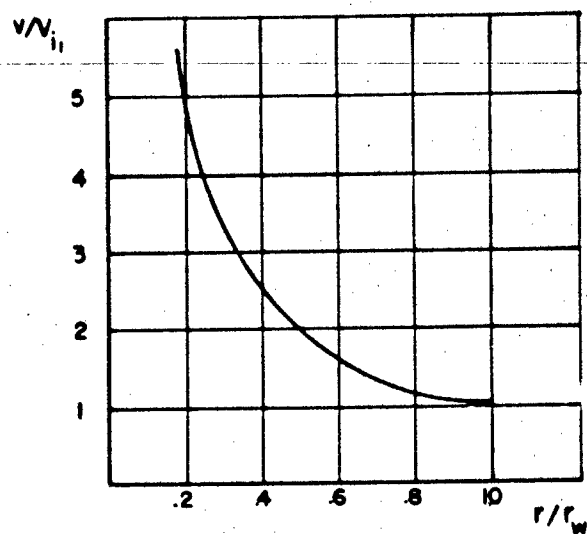
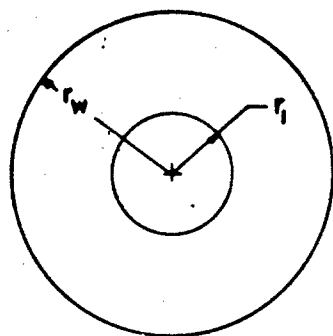
## BIBLIOGRAPHY

6. Ranque, G.J., "Experience sur la Detente Giratoire avec Productions Simultanees d'un Echappement d'air Chaud et d'air Froid," Journal de Physique et de Radium, 1933.
  7. Fulton, C.D., "Ranque's Tube," Journal of the ASRE, Refrigerating Engineering, Vol. 58, 1950, pp. 473-479.
  8. Webster, D.S., "An Analysis of the Hilsch Vortex Tube," Refrigerating Engineering, Vol. 58, 1950, pp. 163-170.
  9. Grunow-Schultz, F., "How the Ranque-Hilsch Vortex Tube Operates," Refrigerating Engineering, Vol. 59, 1951, pp. 52-53.
  10. Foa, J.V., "Crypto-Steady Energy Exchange," Rensselaer Polytechnic Institute, Technical Report TR AE 6202, March 1962; also "A Method of Energy Exchange," ARS Journal, 32, pp. 1396-1498, September 1962.
- 
11. Sibulkin, M., "Unsteady, Viscous, Circular Flow, Part 3. Application to the Ranque-Hilsch Vortex Tube," Journal of Fluid Mechanics, 12, pp. 269-293, 1962.



VORTEX TUBE

FIG.I-1



FREE VORTEX

FIG.I-2

FIG. I-3

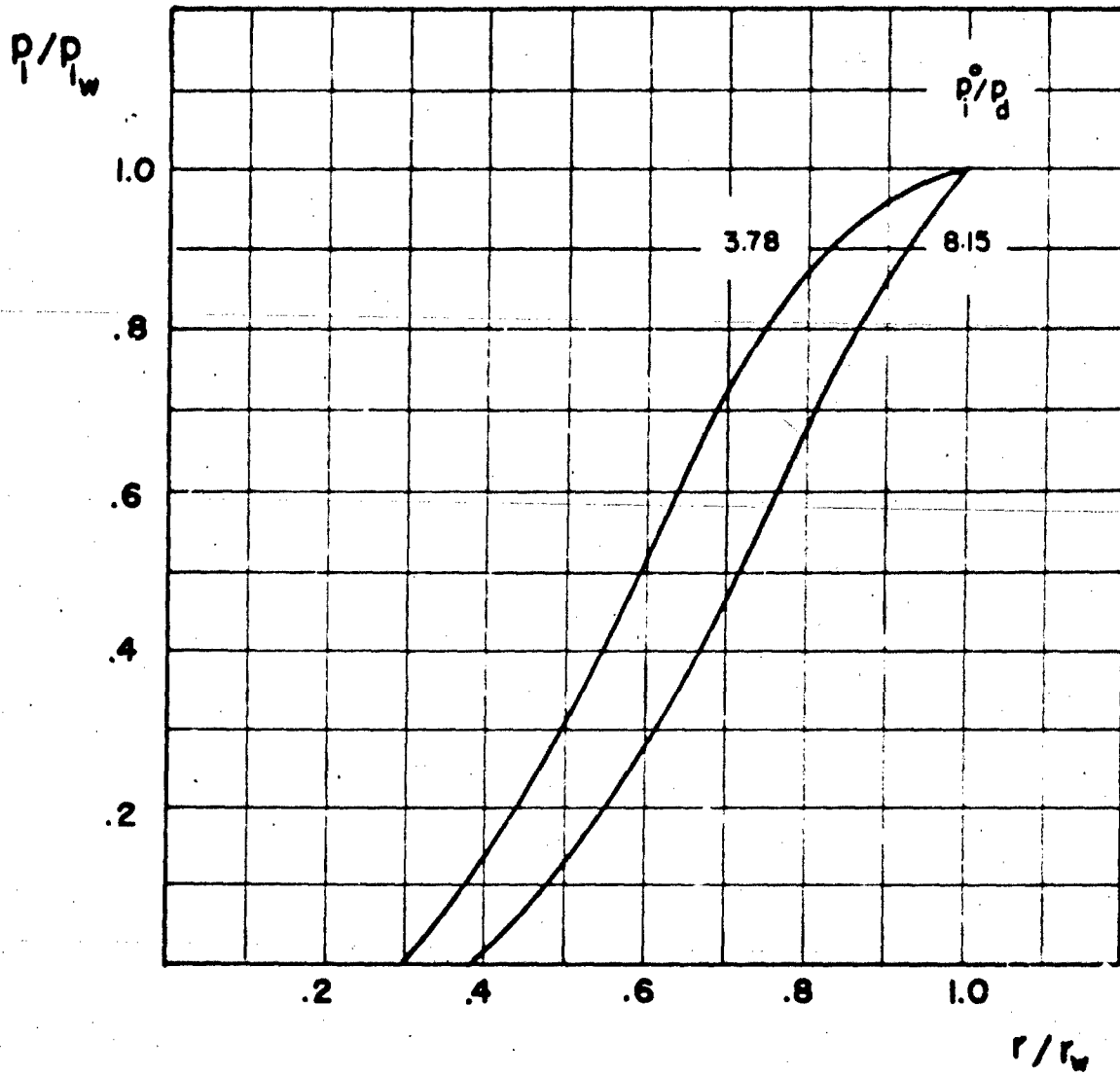


FIG.I-4

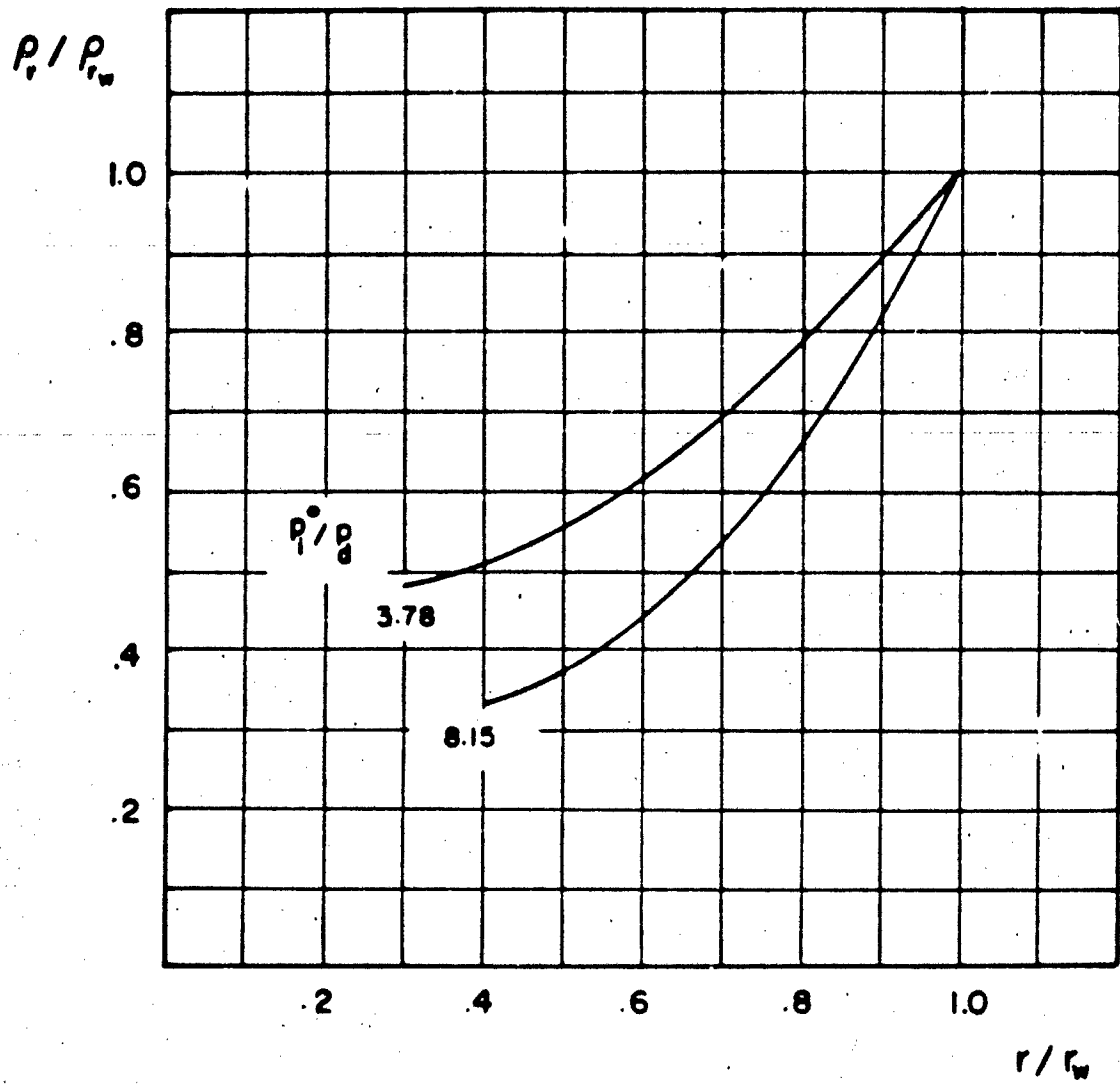
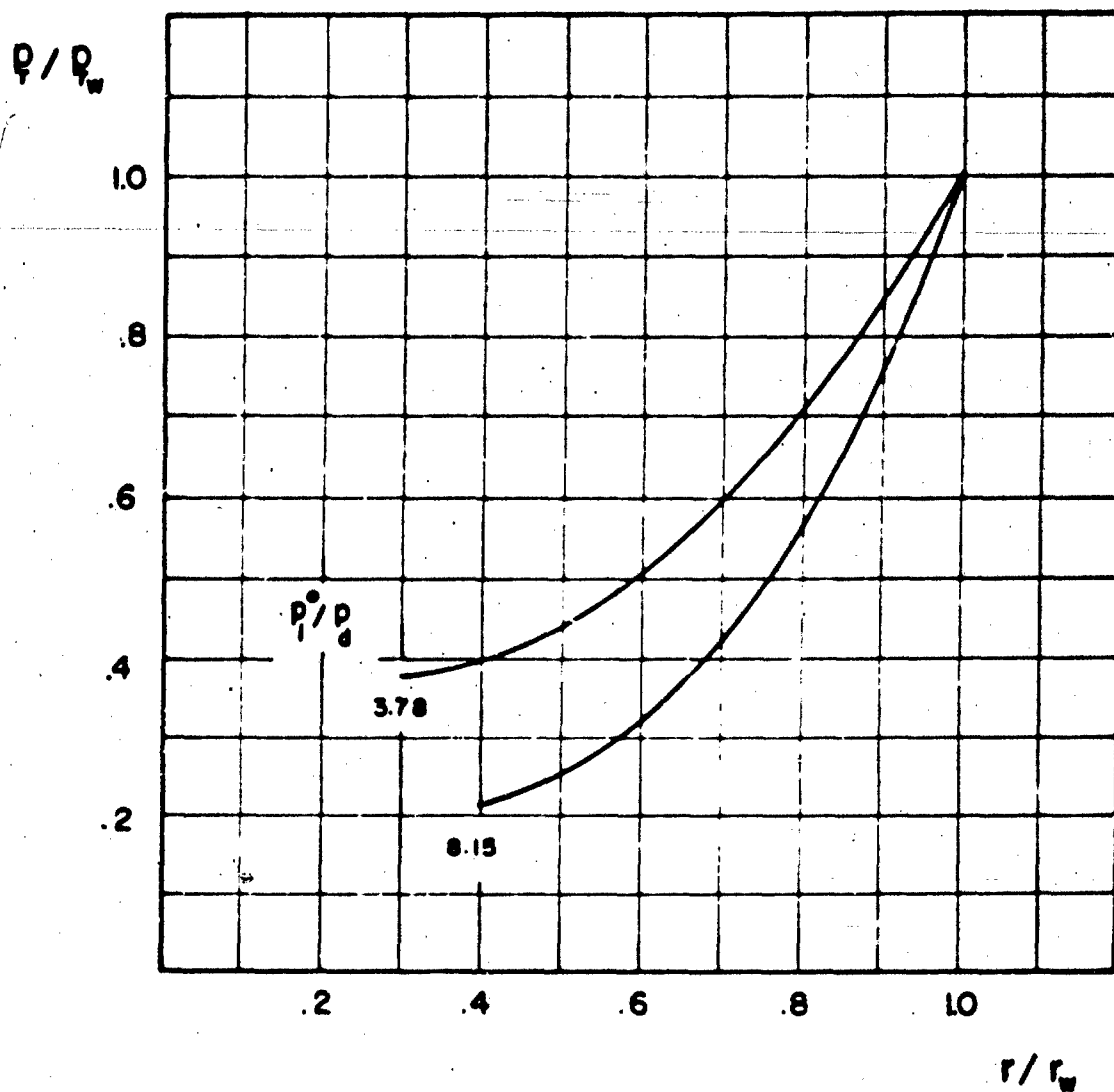




FIG.I-5



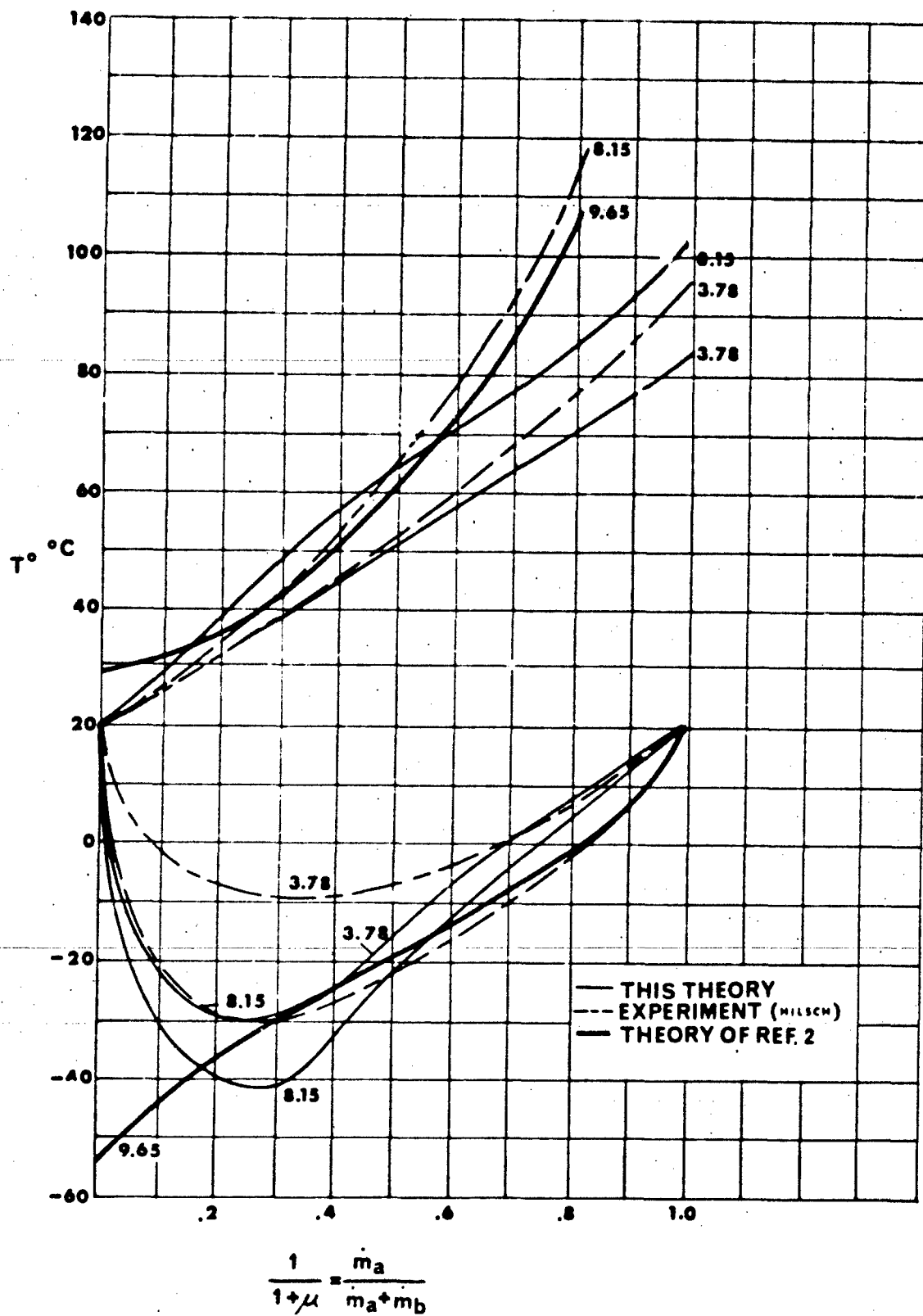


FIG. I-6

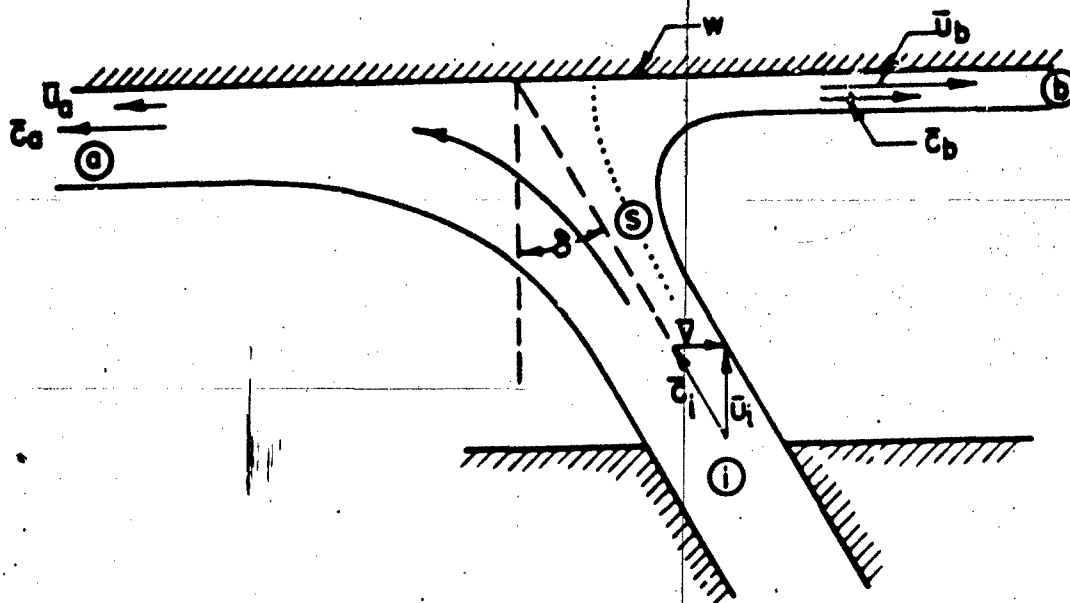


FIG. II-1a

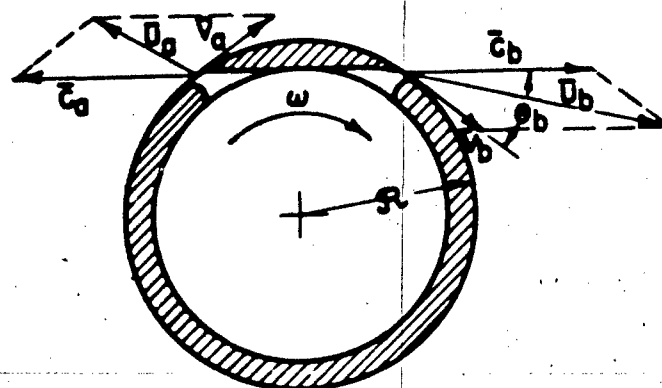


FIG. II-1b

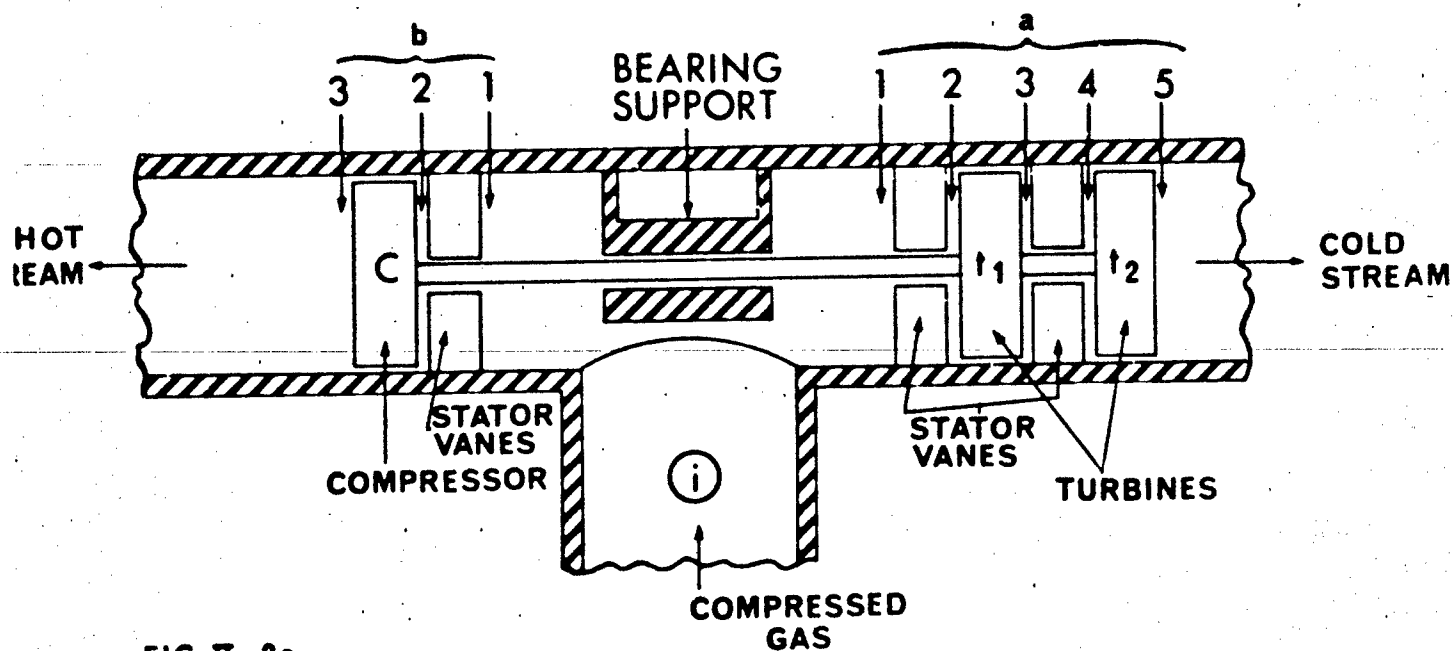


FIG. II-2a

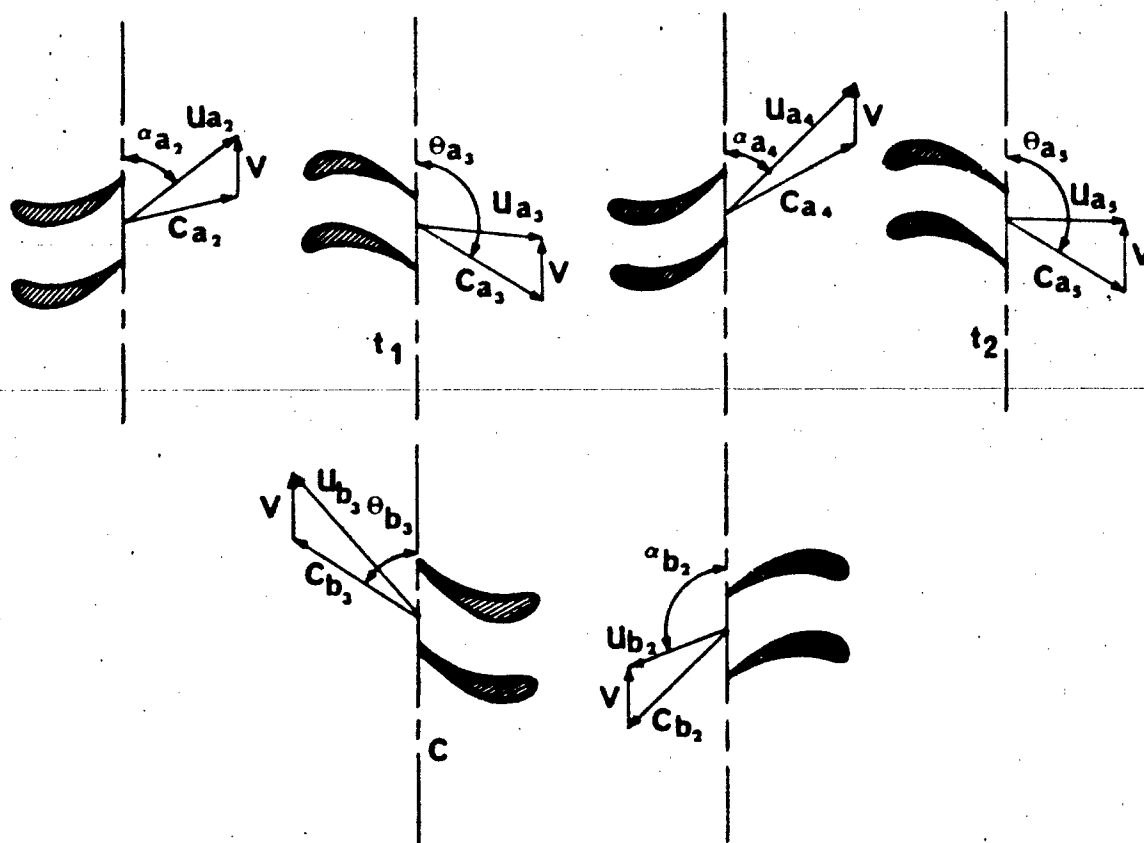
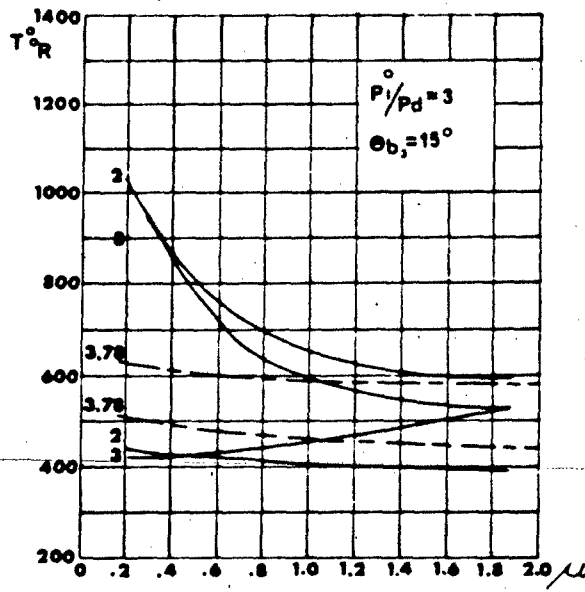
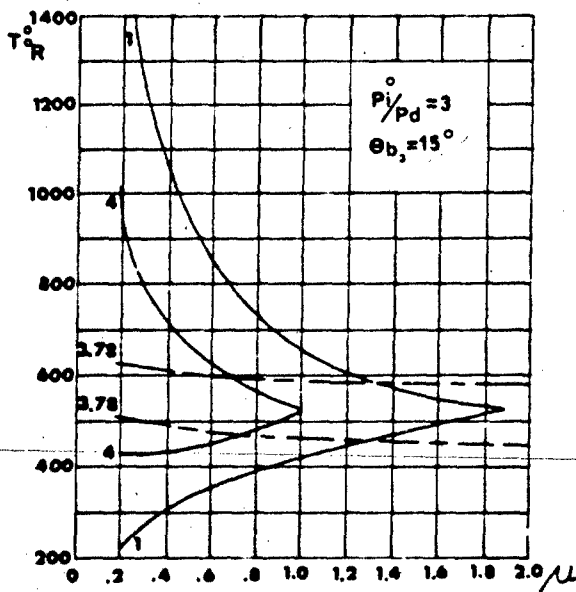
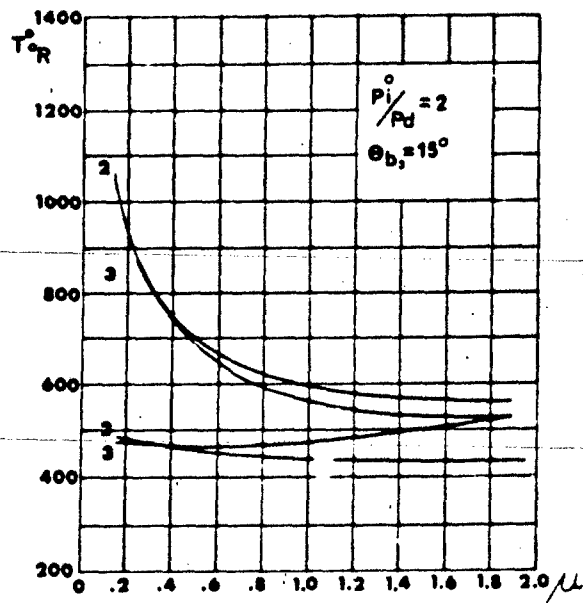
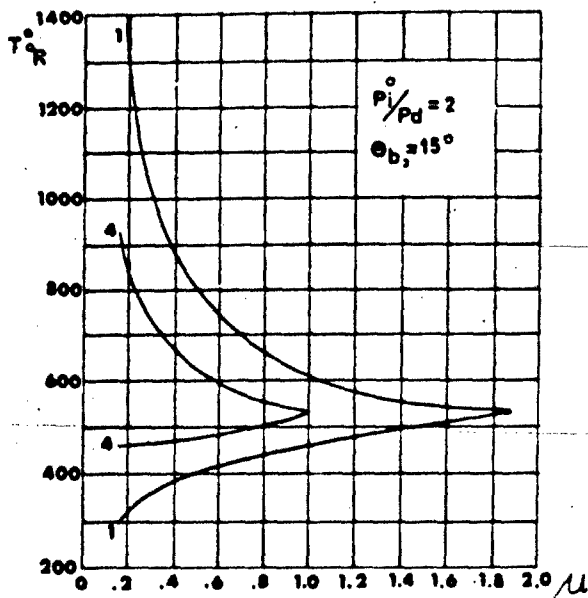


FIG. II-2b

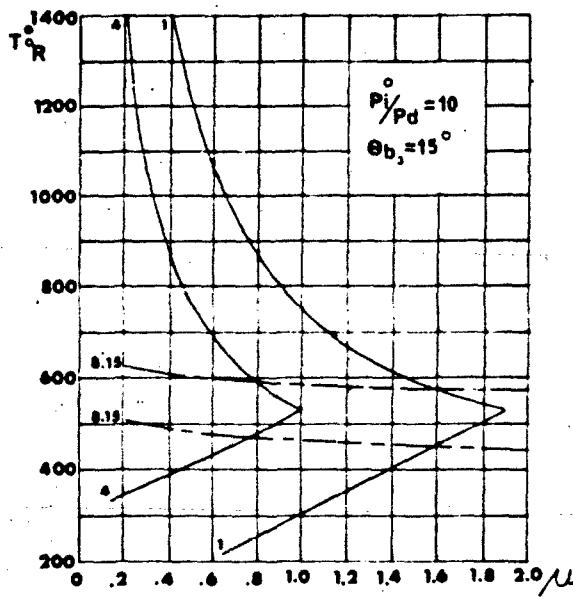
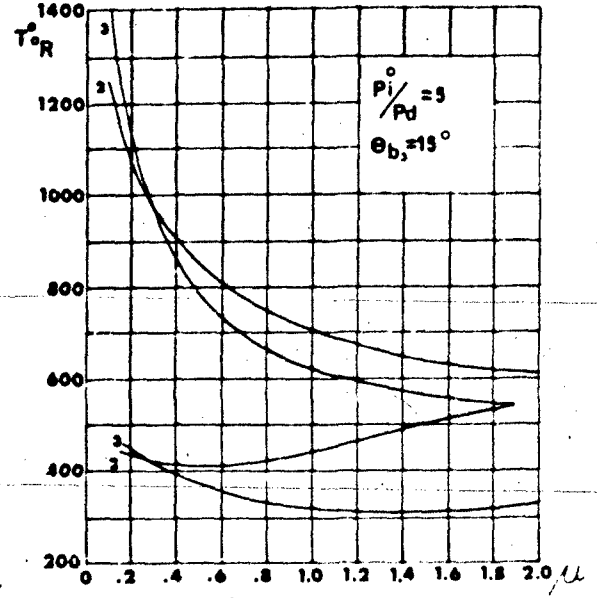
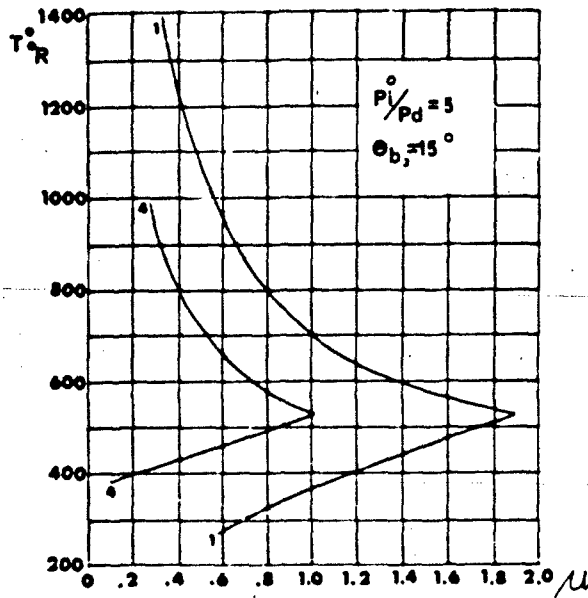
FIG. II-3



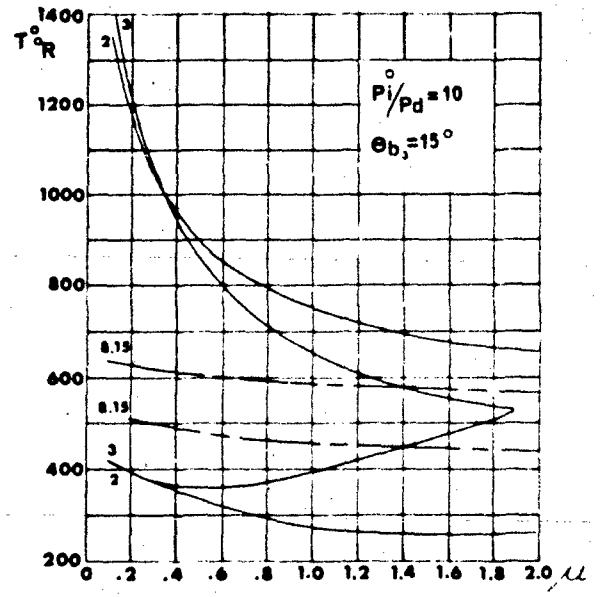
CASE 1 =  $\alpha_{a_4} = 30^\circ$   
CASE 4 =  $\alpha_{a_2} = \alpha_{b_2} = \alpha_{a_4} = 90^\circ$

CASE 2 =  $\alpha_{a_2} = \alpha_{b_2} = 30^\circ$   
CASE 3 =  $\alpha_{a_2} = 30^\circ$

FIG. II-4

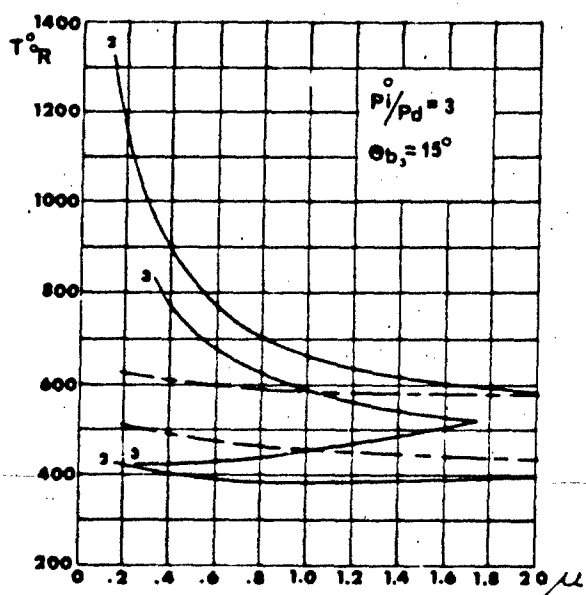
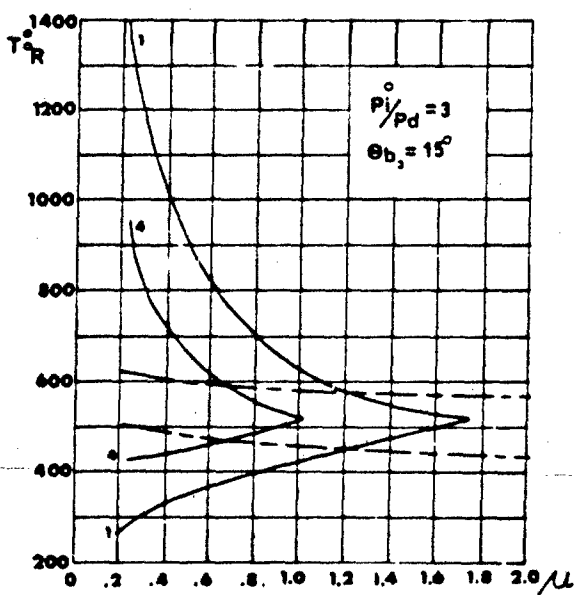
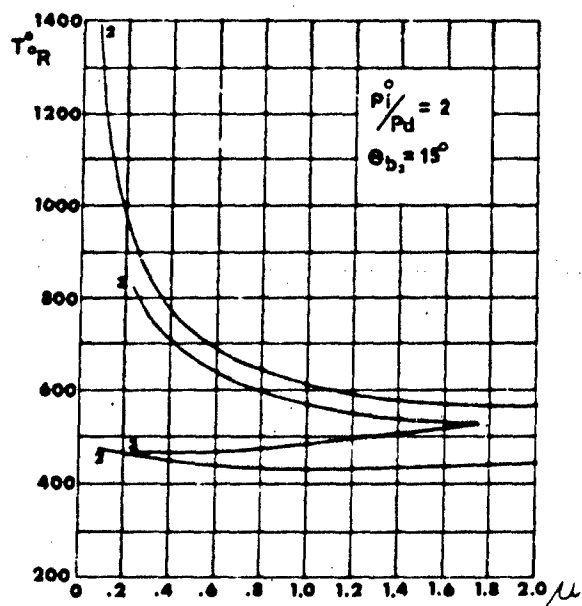
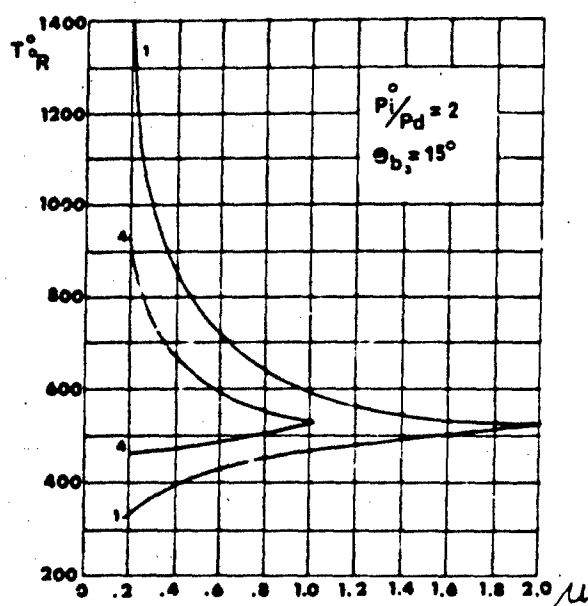


CASE 1 =  $\alpha_a = 30^\circ$   
CASE 4 =  $\alpha_a = \alpha_b = \alpha_c = 90^\circ$



CASE 2 =  $\alpha_a = \alpha_b = 30^\circ$   
CASE 3 =  $\alpha_a = 30^\circ$

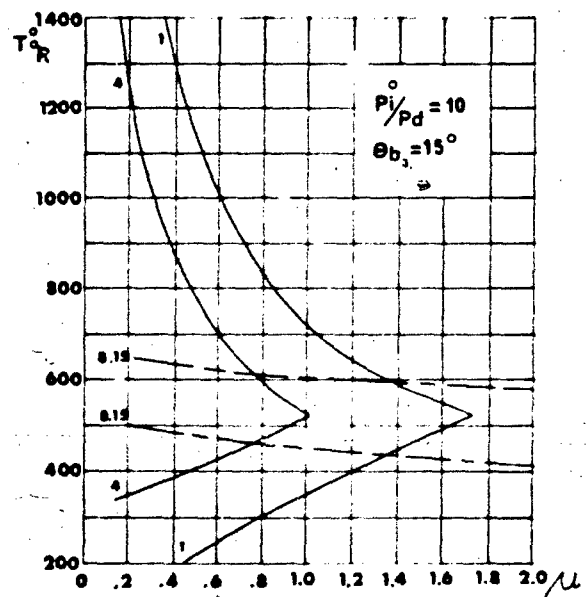
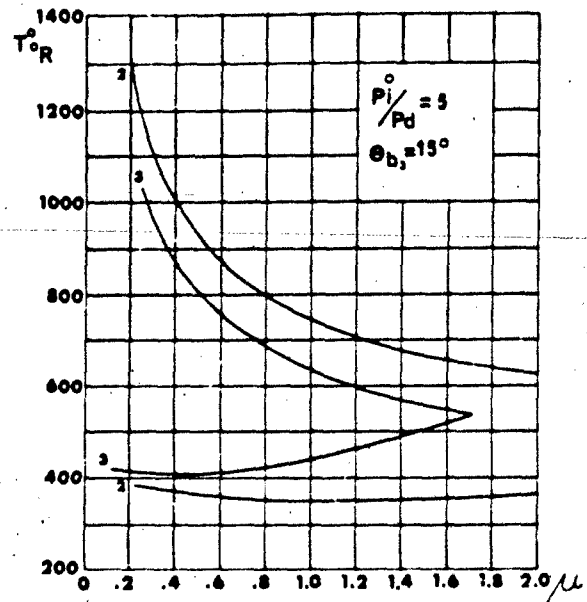
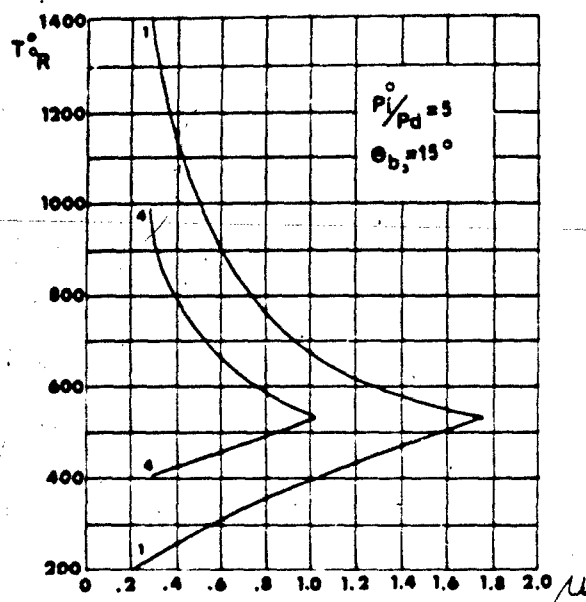
FIG. II-5



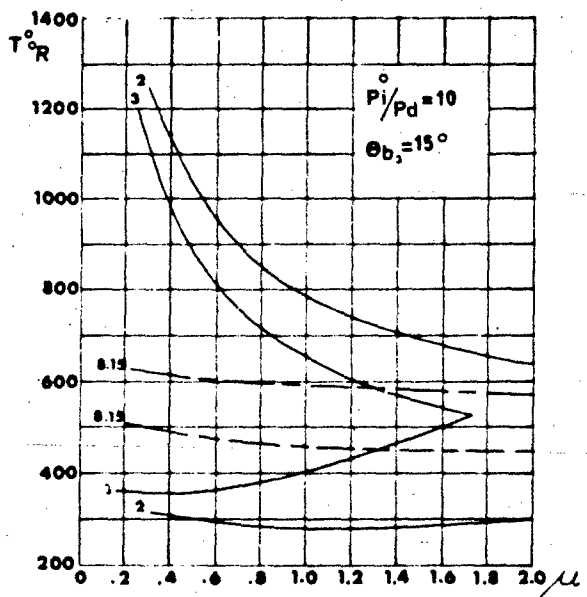
CASE 1 =  $\alpha_a = 45^\circ$   
CASE 4 =  $\alpha_a = \alpha_b = \alpha_c = 90^\circ$

CASE 2 =  $\alpha_a = \alpha_b = 45^\circ$   
CASE 3 =  $\alpha_a = 45^\circ$

FIG. II-6



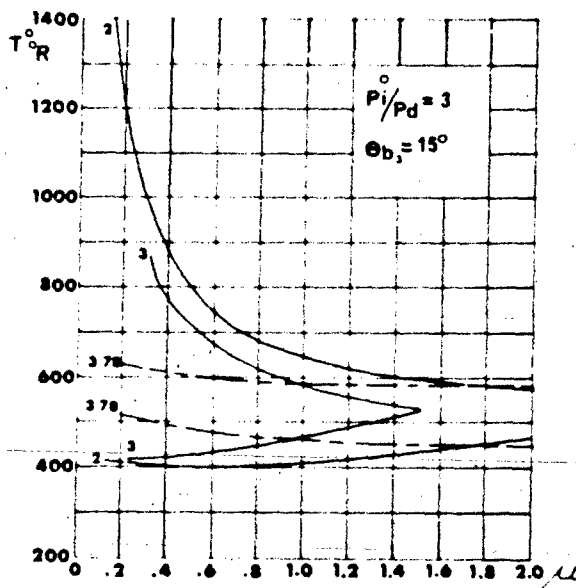
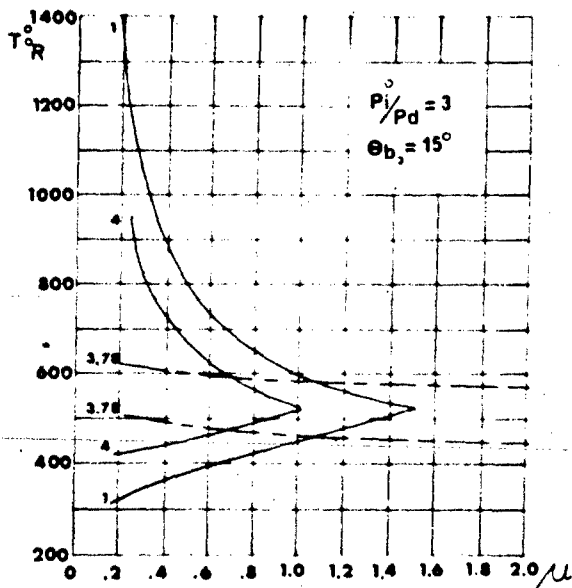
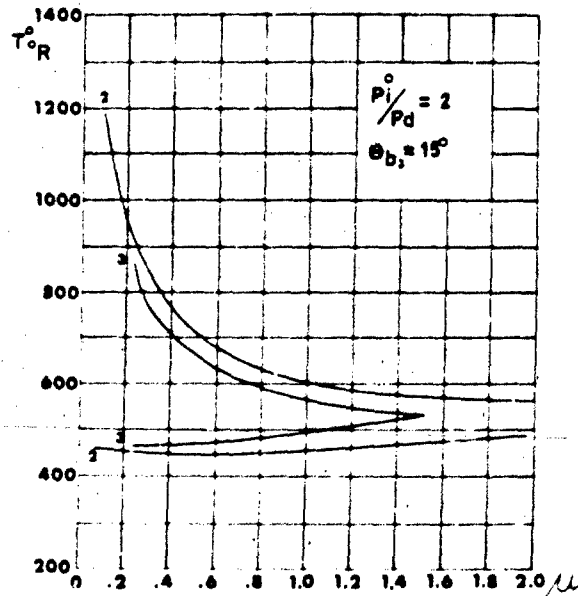
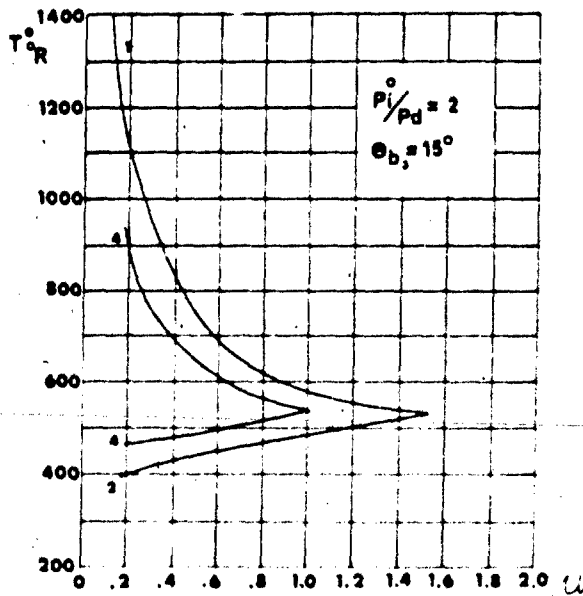
CASE 1 =  $\alpha_{a_1} = 45^\circ$   
CASE 4 =  $\alpha_{a_1} = \alpha_{b_1} = \alpha_{a_2} = 90^\circ$



CASE 2 =  $\alpha_{a_1} = \alpha_{b_1} = 45^\circ$   
CASE 3 =  $\alpha_{a_1} = 45^\circ$



FIG. II-7



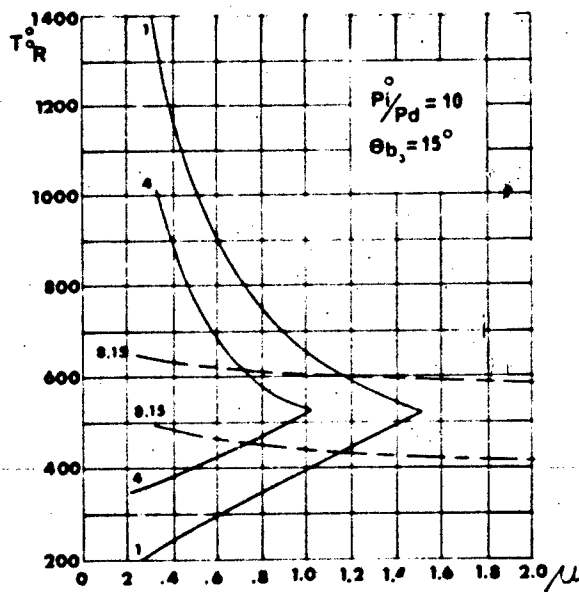
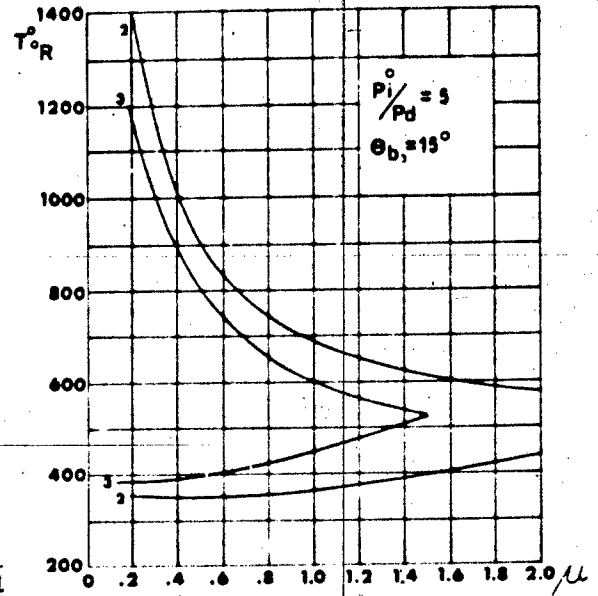
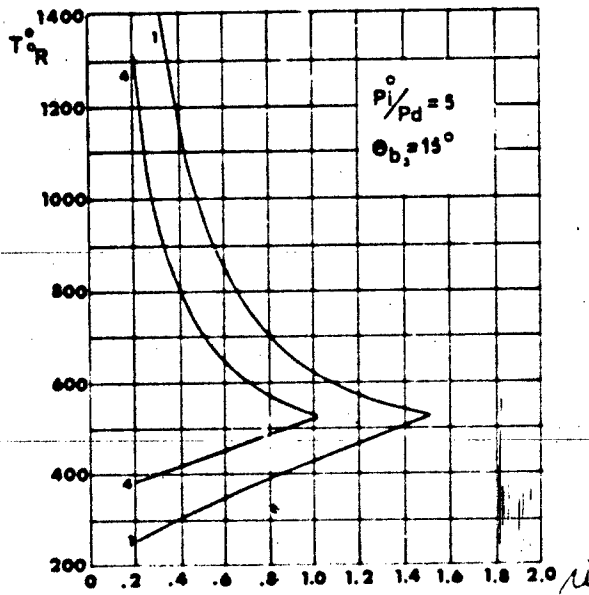
CASE 1 =  $\alpha_a = 60^{\circ}$

CASE 4 =  $\alpha_a = \alpha_b = \alpha_s = 90^{\circ}$

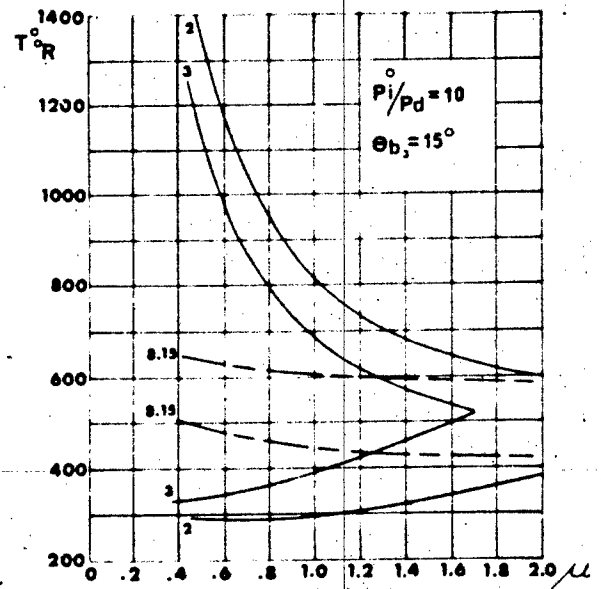
CASE 2 =  $\alpha_a = \alpha_b = 60^{\circ}$

CASE 3 =  $\alpha_a = 60^{\circ}$

FIG. II-8

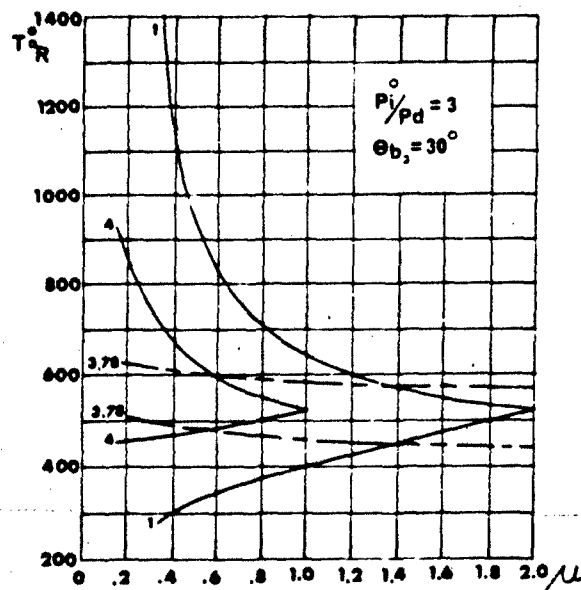
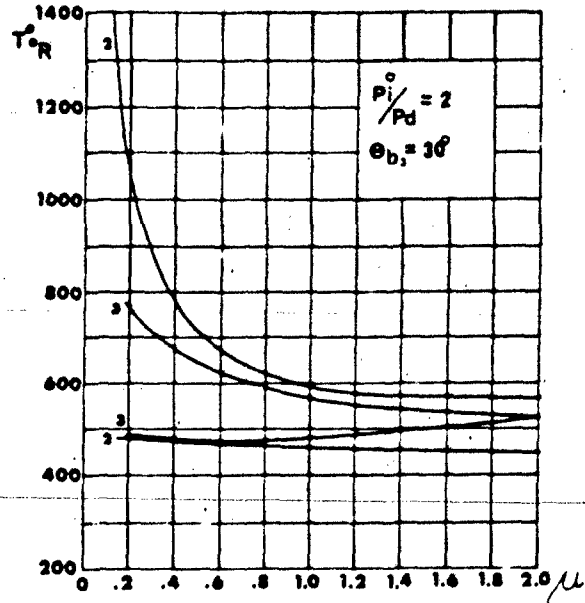
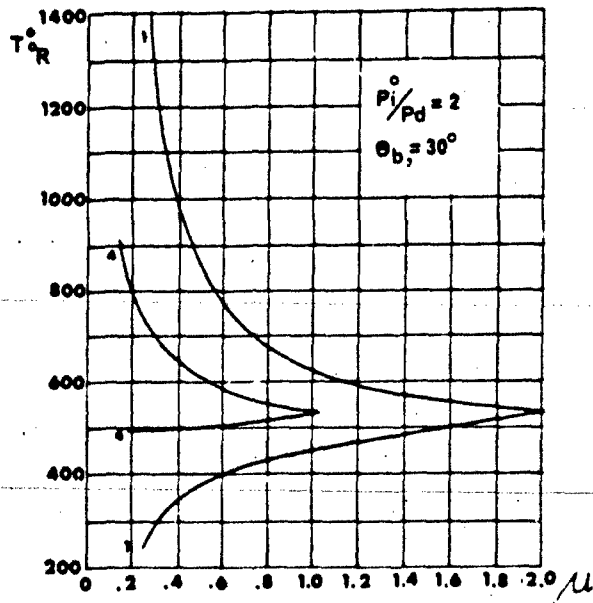


CASE 1 =  $\alpha_a = 60^{\circ}$   
CASE 4 =  $\alpha_a = \alpha_b = \alpha_c = 90^{\circ}$

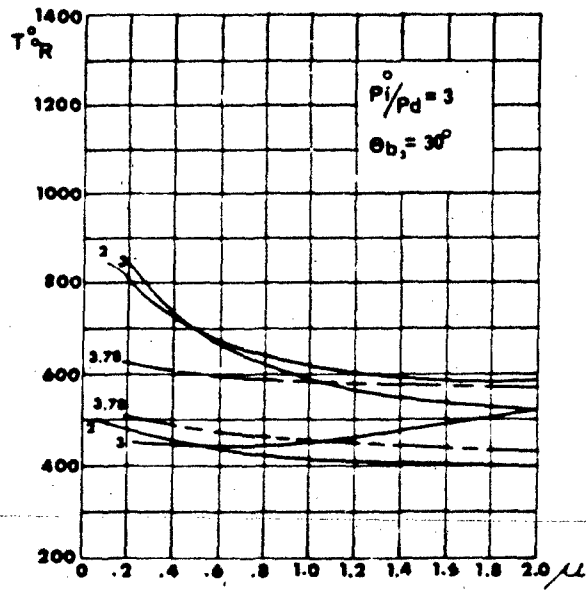


CASE 2 =  $\alpha_a = \alpha_b = 60^{\circ}$   
CASE 3 =  $\alpha_a = 60^{\circ}$

FIG. II-9

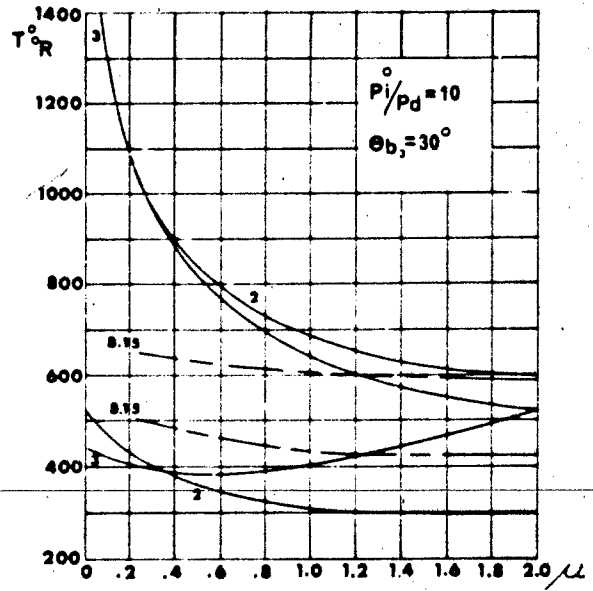
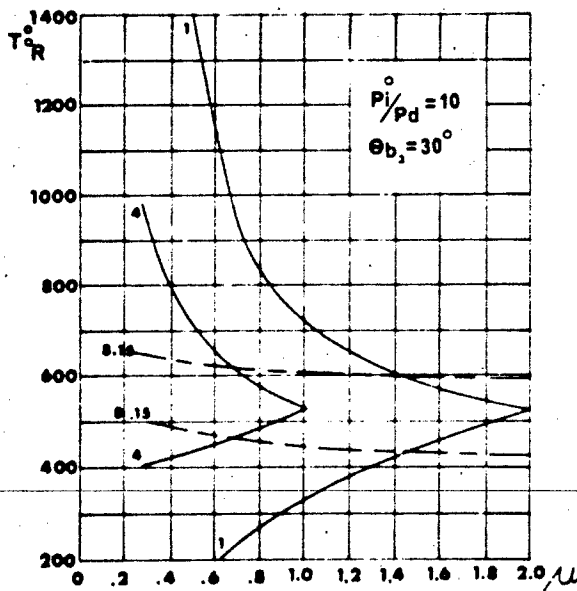
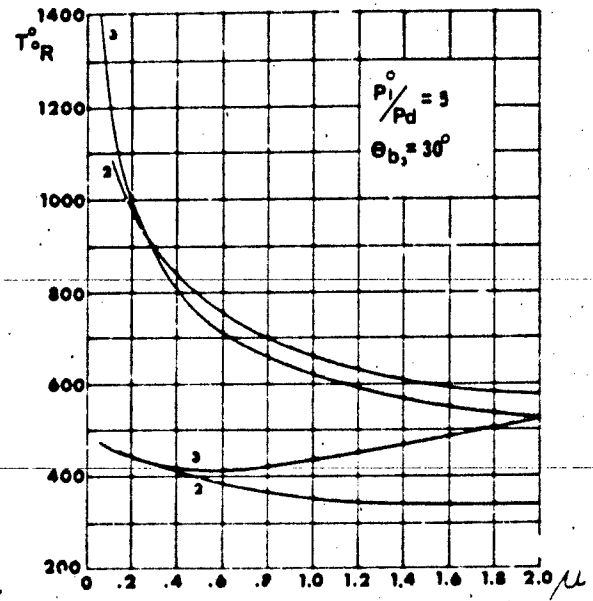
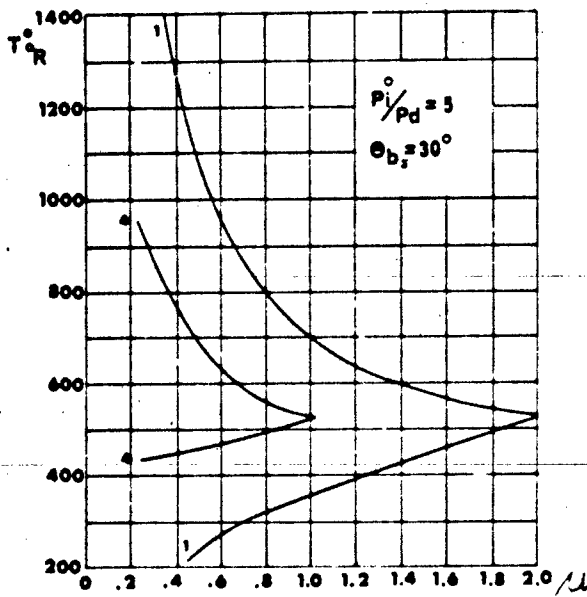


CASE 1 =  $\alpha_a = 30^{\circ}$   
CASE 4 =  $\alpha_a = \alpha_b = \alpha_a = 90^{\circ}$



CASE 2 =  $\alpha_a = \alpha_b = 30^{\circ}$   
CASE 3 =  $\alpha_a = 30^{\circ}$

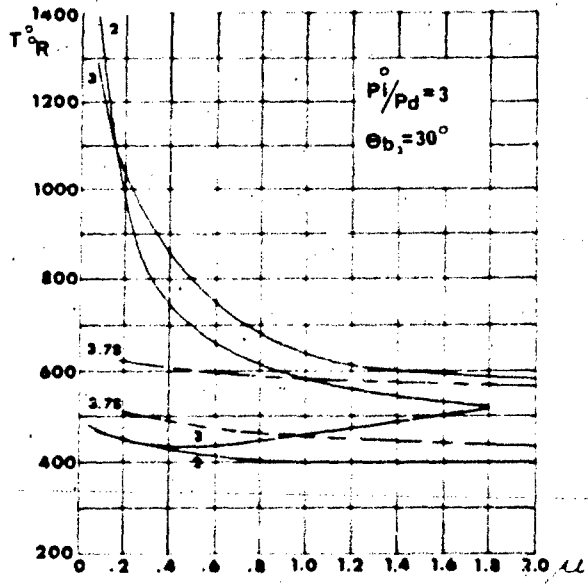
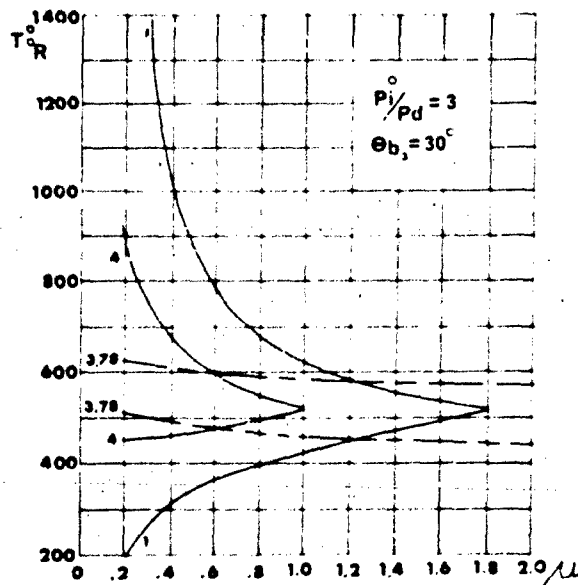
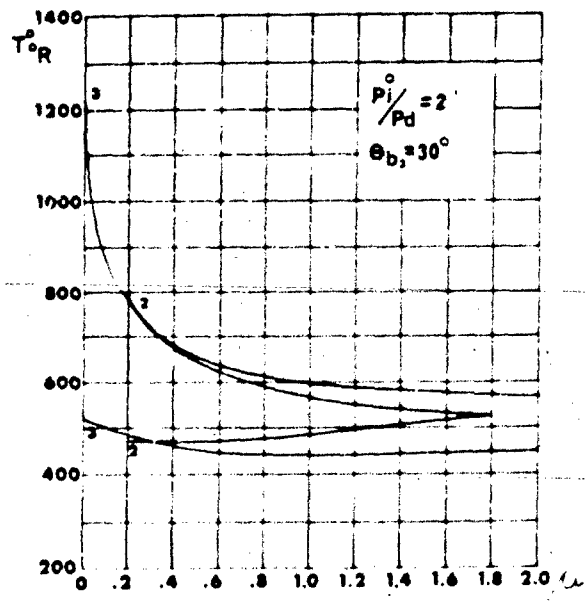
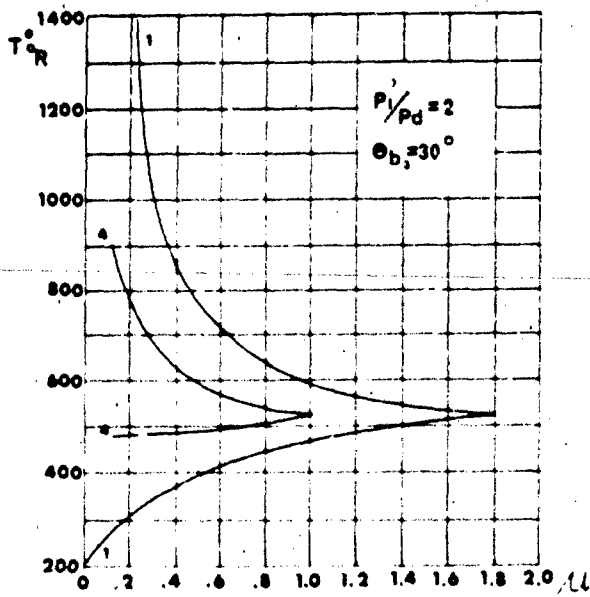
FIG. II-10



CASE 1 =  $\alpha_{a1} = 30^{\circ}$   
CASE 4 =  $\alpha_{a1} = \alpha_{b1} = \alpha_{a2} = 90^{\circ}$

CASE 2 =  $\alpha_{a1} = \alpha_{b1} = 30^{\circ}$   
CASE 3 =  $\alpha_{a1} = 30^{\circ}$

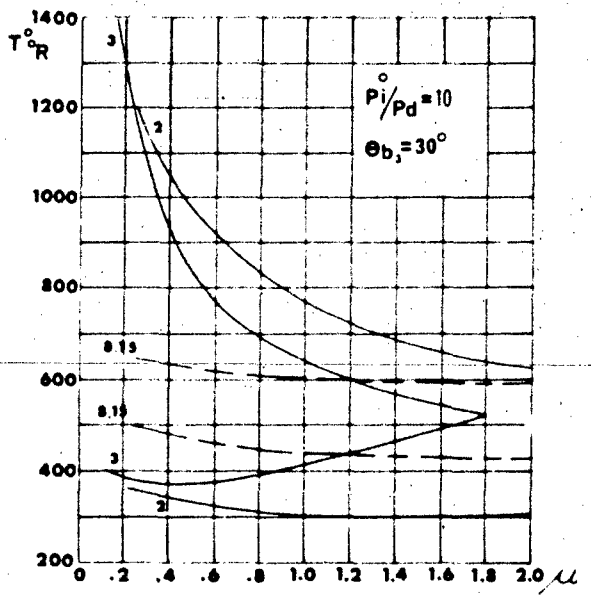
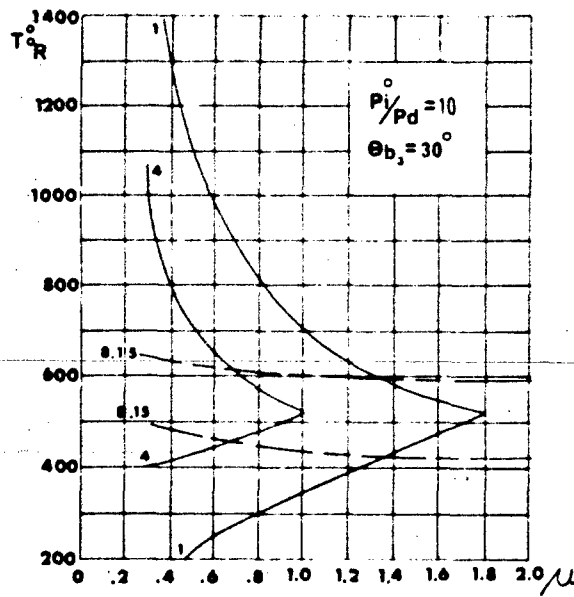
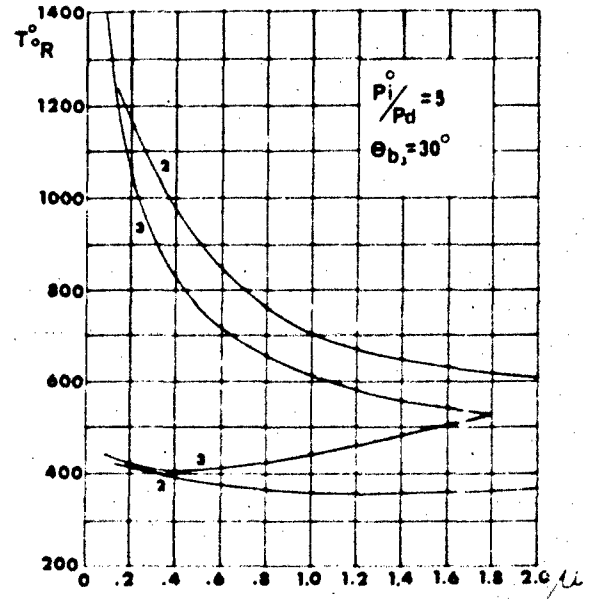
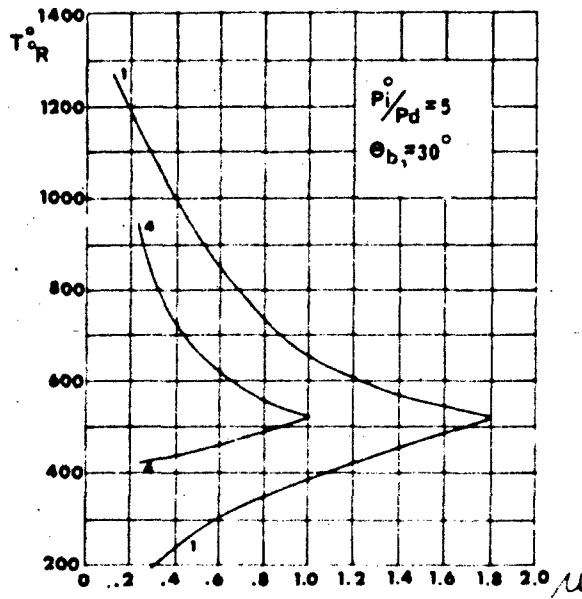
FIG. II-11



CASE 1 =  $\alpha_{a1} = 45^{\circ}$   
CASE 4 =  $\alpha_{a1} = \alpha_{b1} = \alpha_{a2} = 90^{\circ}$

CASE 2 =  $\alpha_{a1} = \alpha_{b1} = 45^{\circ}$   
CASE 3 =  $\alpha_{a1} = 45^{\circ}$

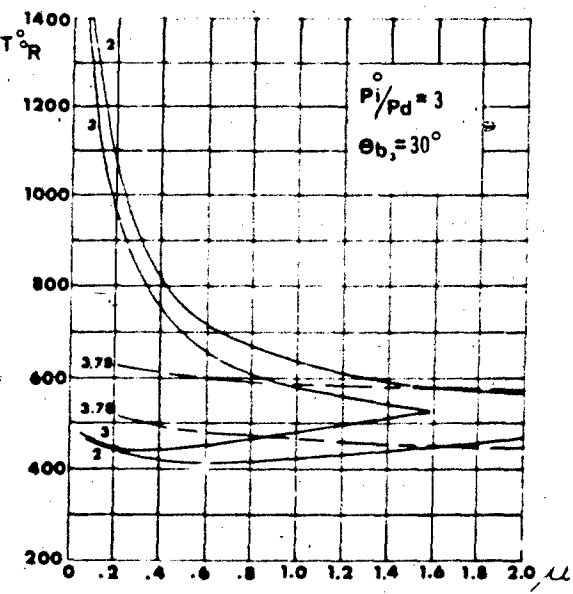
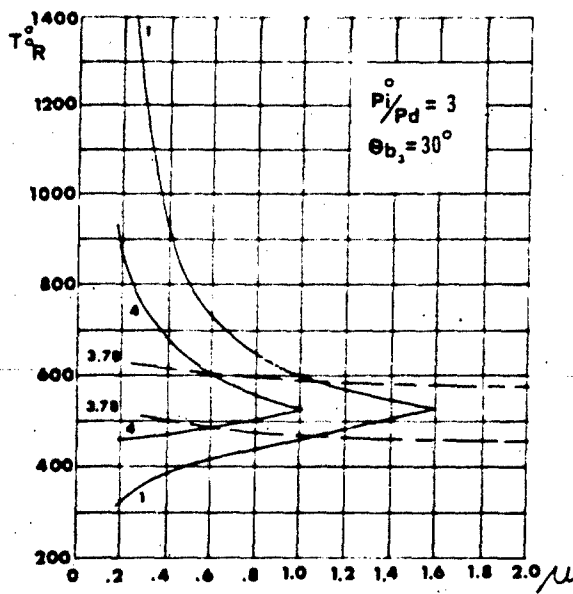
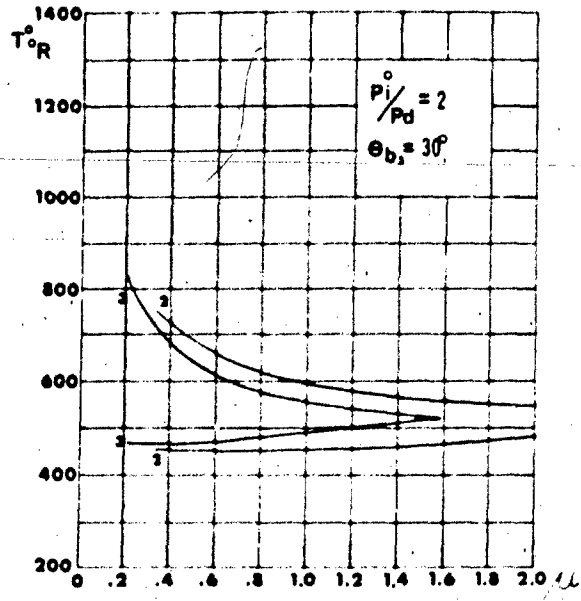
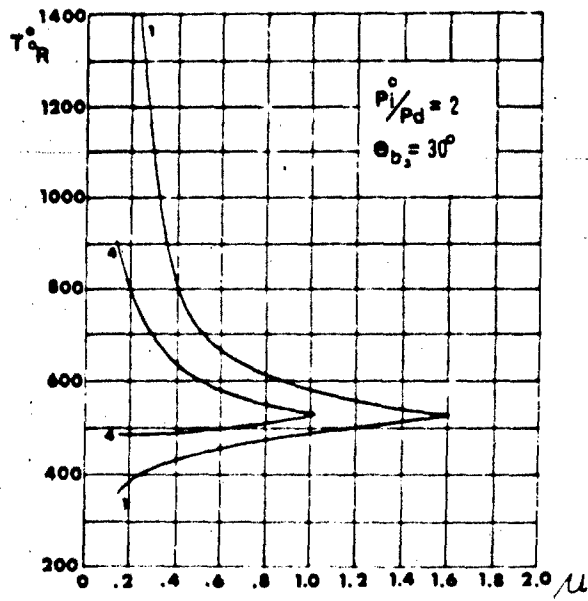
FIG. II-12



CASE 1 =  $\alpha_{a1} = 45^{\circ}$   
CASE 4 =  $\alpha_{a1} = \alpha_{b1} = \alpha_{a2} = 90^{\circ}$

CASE 2 =  $\alpha_{a1} = \alpha_{b1} = 45^{\circ}$   
CASE 3 =  $\alpha_{a1} = 45^{\circ}$

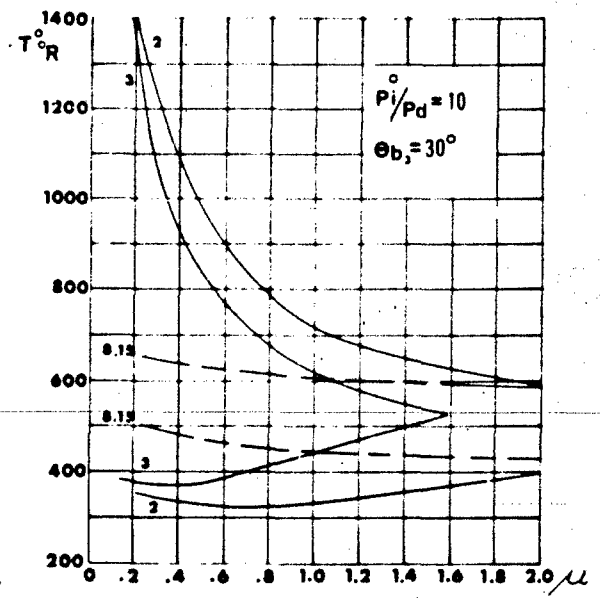
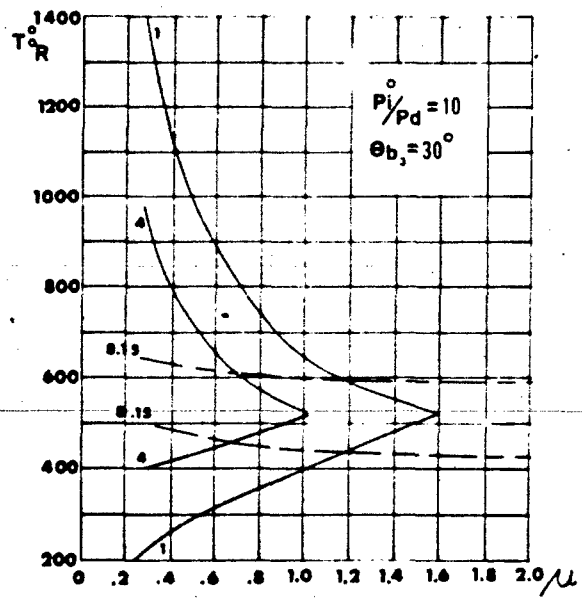
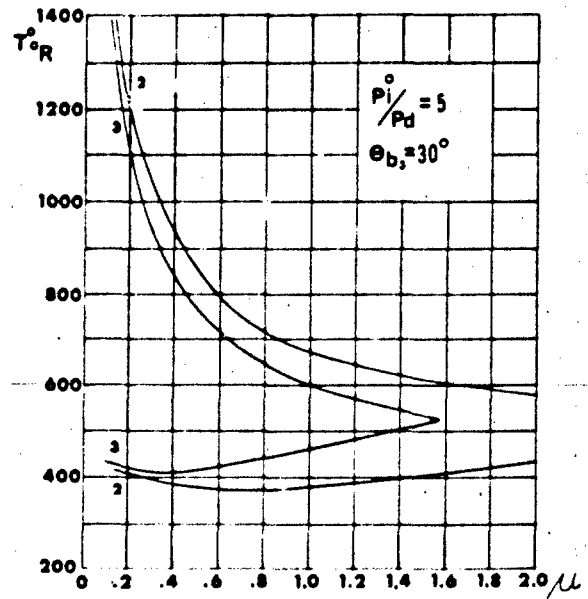
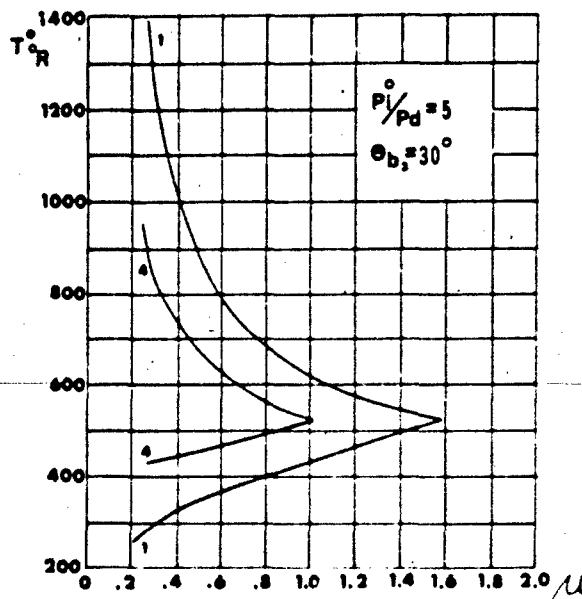
FIG. II - 13



CASE 1 =  $\alpha_a = 60^{\circ}$   
CASE 4 =  $\alpha_a = \alpha_{b1} = \alpha_{a1} = 90^{\circ}$

CASE 2 =  $\alpha_a = \alpha_{b1} = 60^{\circ}$   
CASE 3 =  $\alpha_a = 60^{\circ}$

FIG. II-14

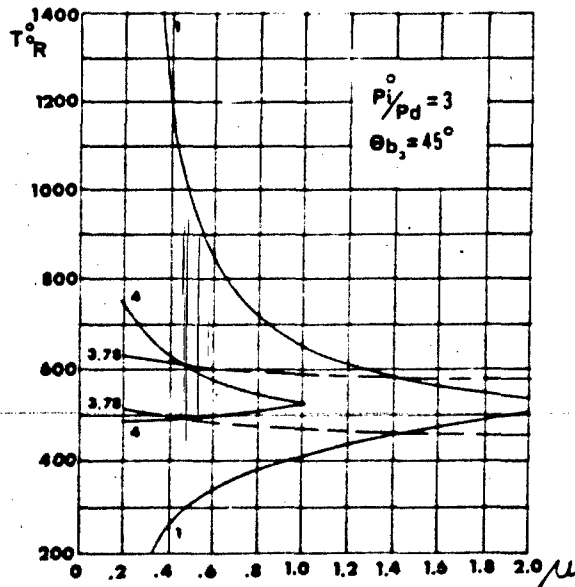
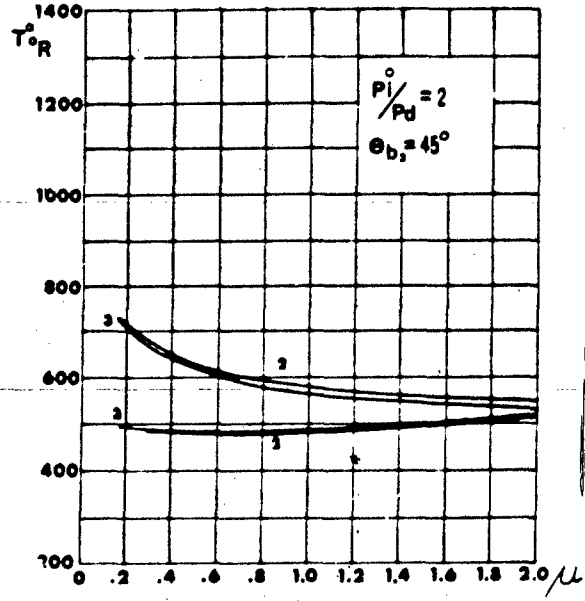
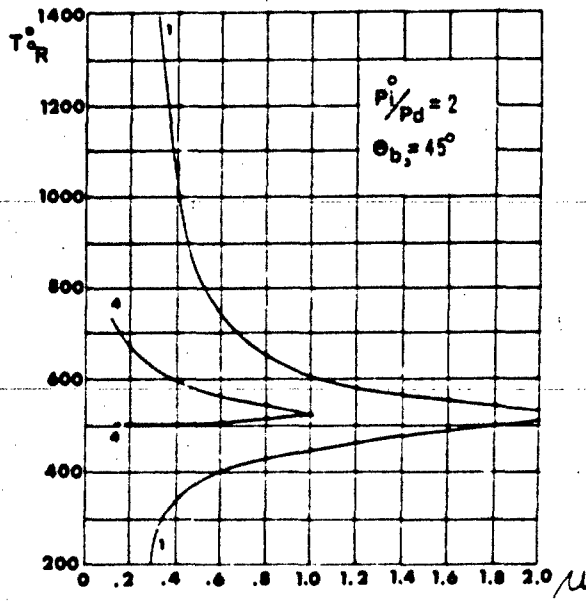


CASE 1 =  $\alpha_{a_1} = 60^\circ$   
CASE 4 =  $\alpha_{a_1} = \alpha_{b_1} = \alpha_{a_2} = 90^\circ$

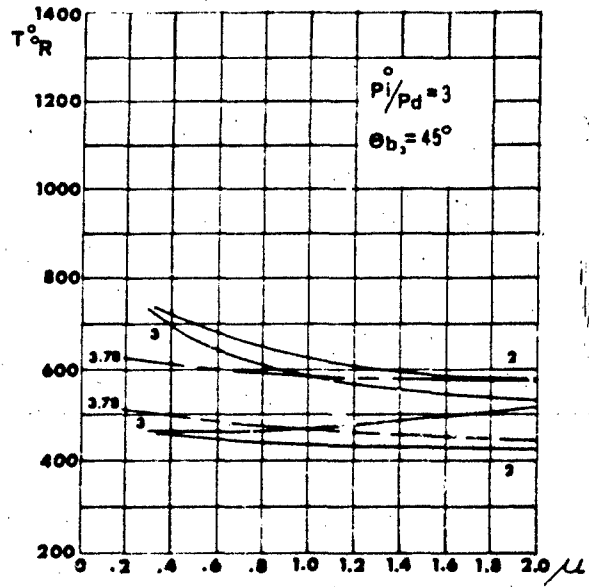
CASE 2 =  $\alpha_{a_1} = \alpha_{b_1} = 60^\circ$   
CASE 3 =  $\alpha_{a_1} = 60^\circ$



FIG. II-15

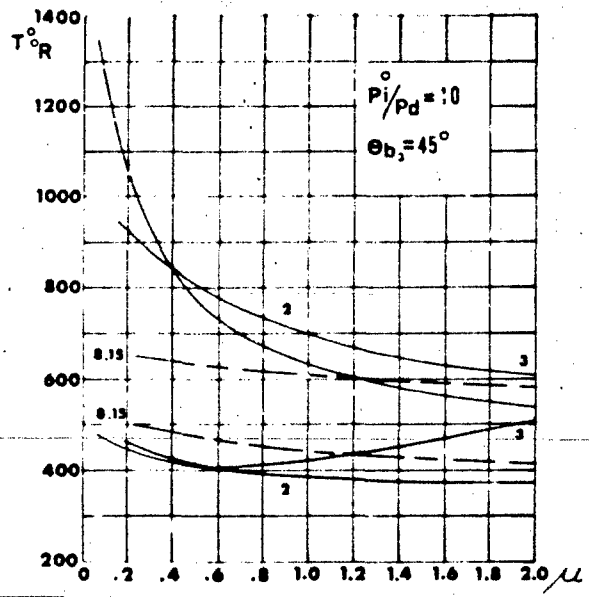
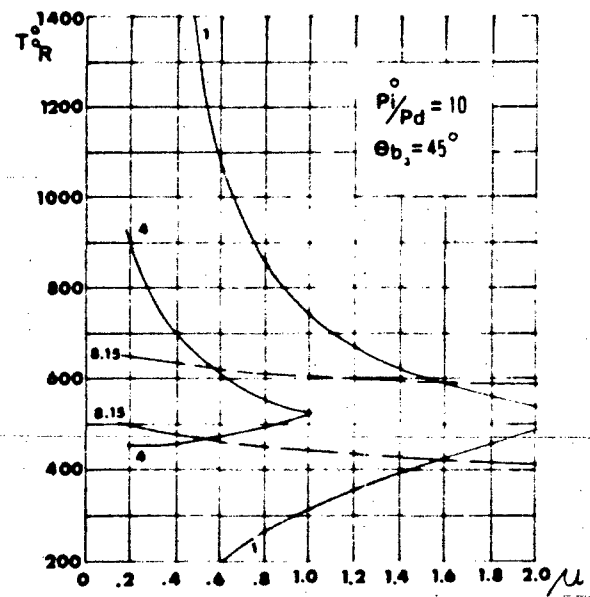
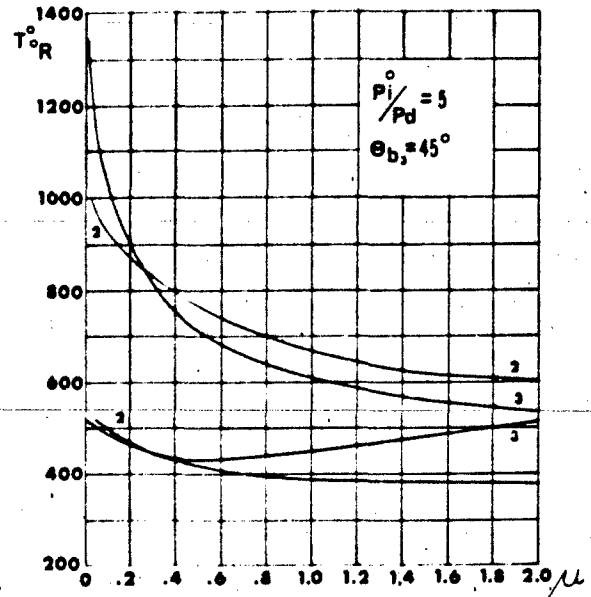
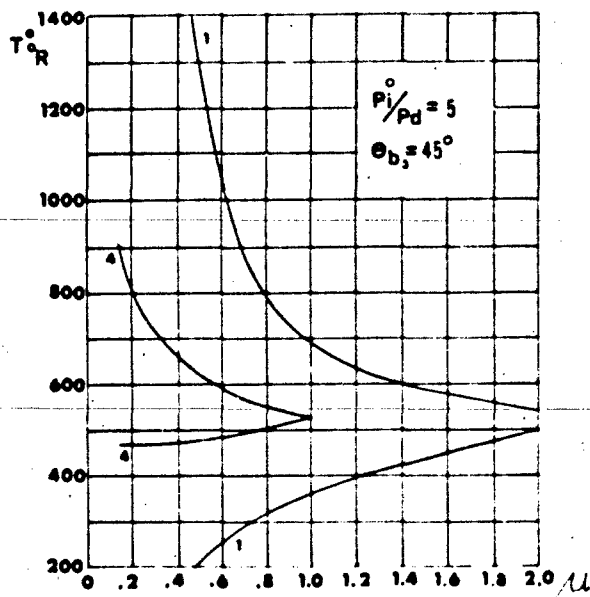


CASE 1 =  $\alpha_a = 30^{\circ}$   
CASE 4 =  $\alpha_a = \alpha_b = \alpha_{a_1} = 90^{\circ}$



CASE 2 =  $\alpha_a = \alpha_b = 30^{\circ}$   
CASE 3 =  $\alpha_a = 30^{\circ}$

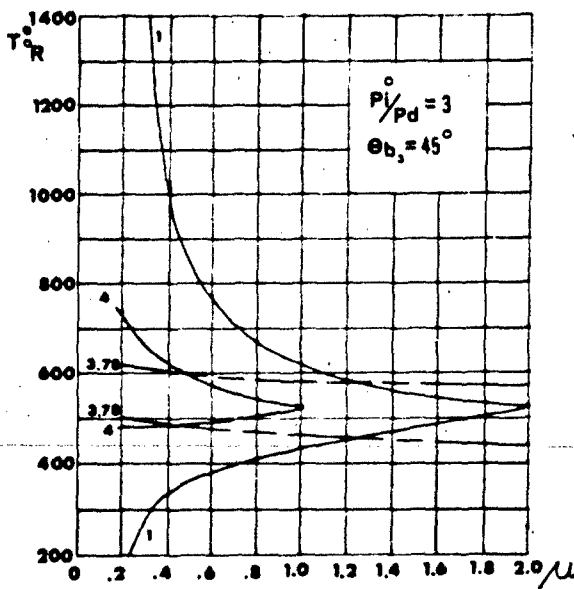
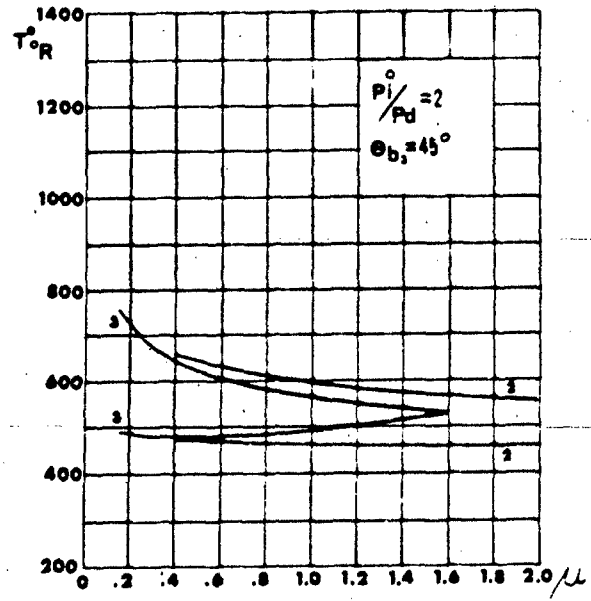
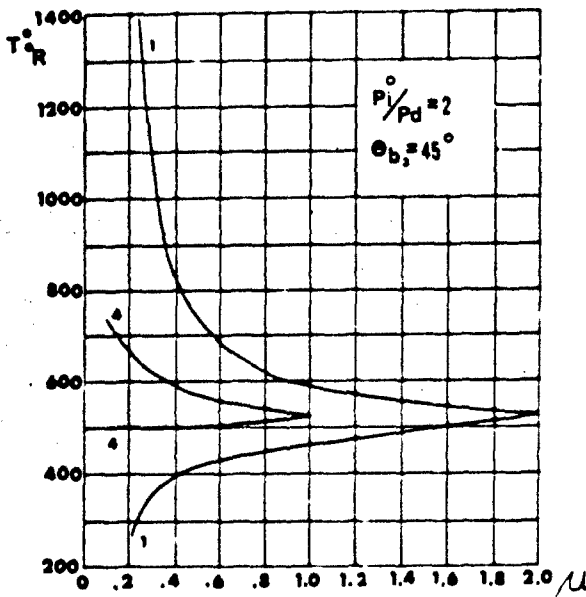
FIG. II-16



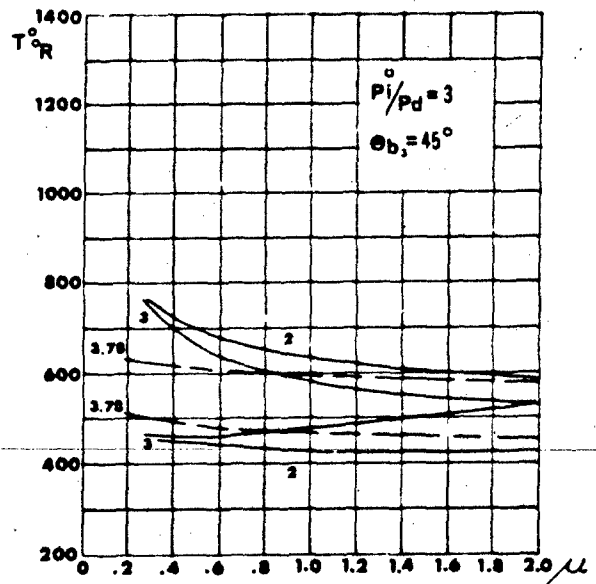
CASE 1 =  $\alpha_{a_j} = 30^{\circ}$   
CASE 4 =  $\alpha_{a_j} = \alpha_{b_j} = \alpha_{a_s} = 90^{\circ}$

CASE 2 =  $\alpha_{a_j} = \alpha_{b_j} = 30^{\circ}$   
CASE 3 =  $\alpha_{a_j} = 30^{\circ}$

FIG. II-17

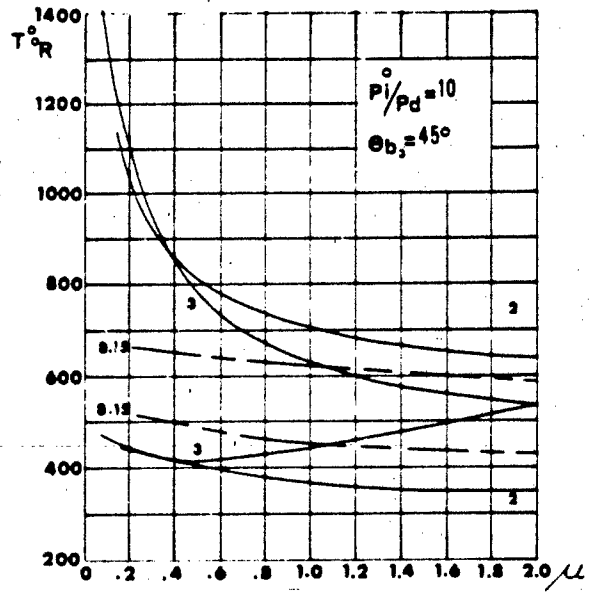
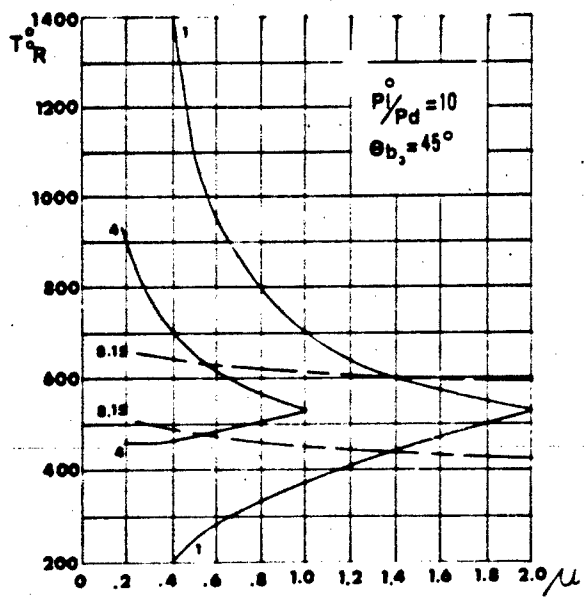
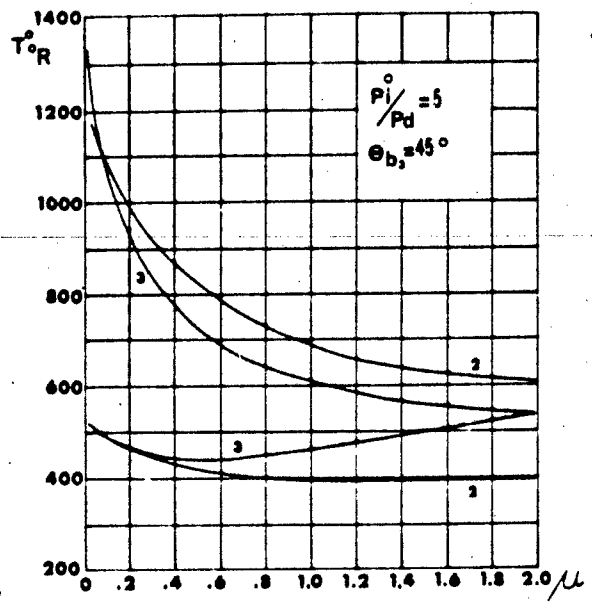
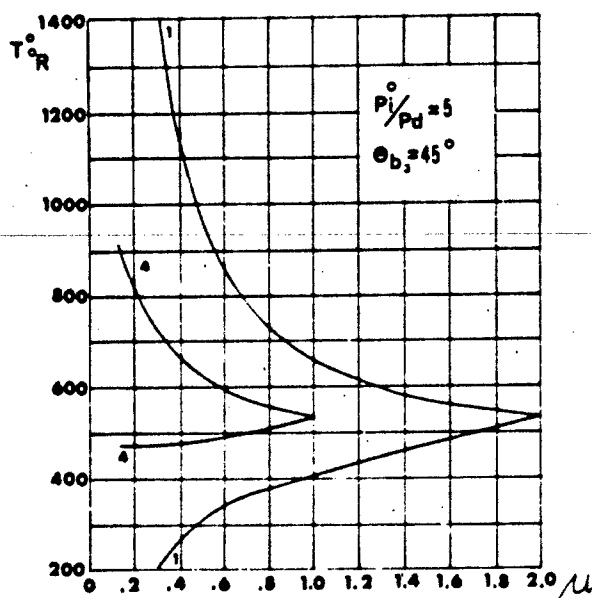


CASE 1 =  $\alpha_{a_1} = 45^{\circ}$   
CASE 4 =  $\alpha_{a_1} = \alpha_{b_1} = \alpha_{a_2} = 90^{\circ}$



CASE 2 =  $\alpha_{a_1} = \alpha_{b_1} = 45^{\circ}$   
CASE 3 =  $\alpha_{a_1} = 45^{\circ}$

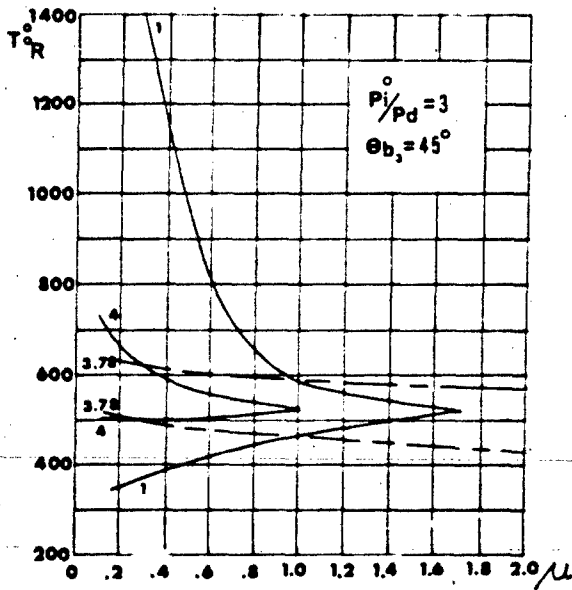
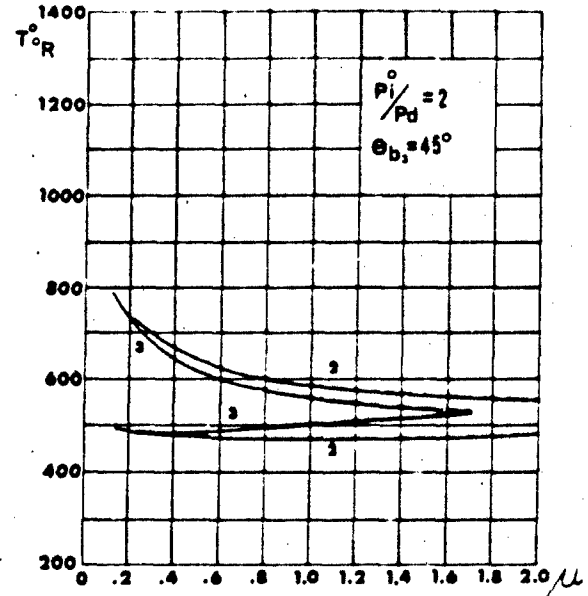
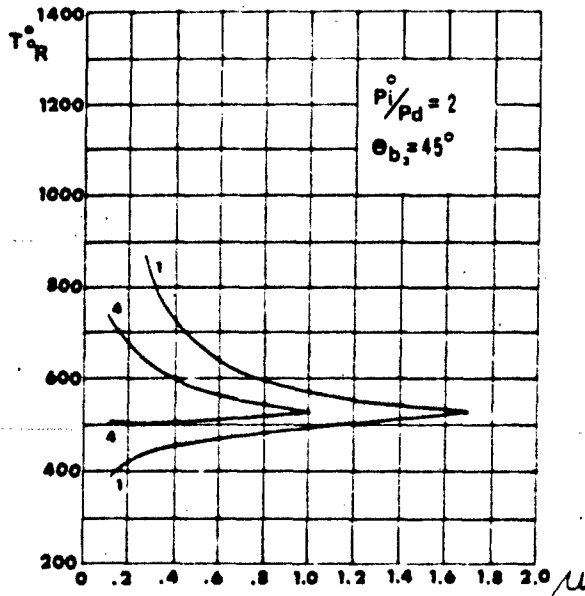
FIG. II-18



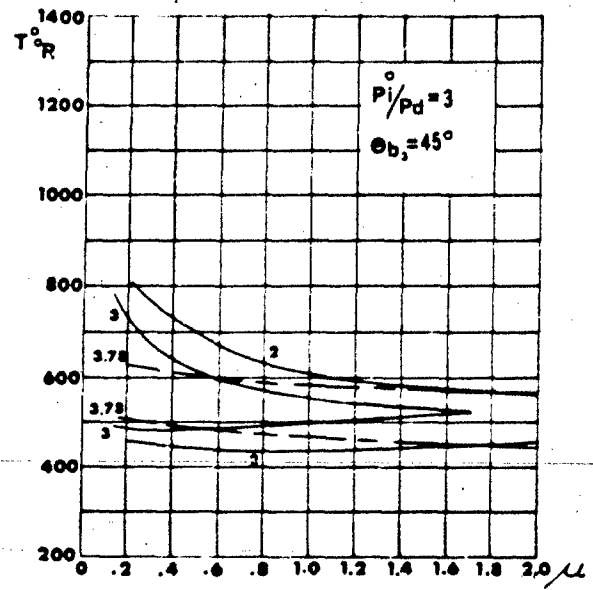
CASE 1 =  $\alpha_{a_1} = 45^{\circ}$   
CASE 4 =  $\alpha_{a_1} = \alpha_{b_1} = \alpha_{a_2} = 90^{\circ}$

CASE 2 =  $\alpha_{a_1} = \alpha_{b_1} = 45^{\circ}$   
CASE 3 =  $\alpha_{a_1} = 45^{\circ}$

FIG II-19

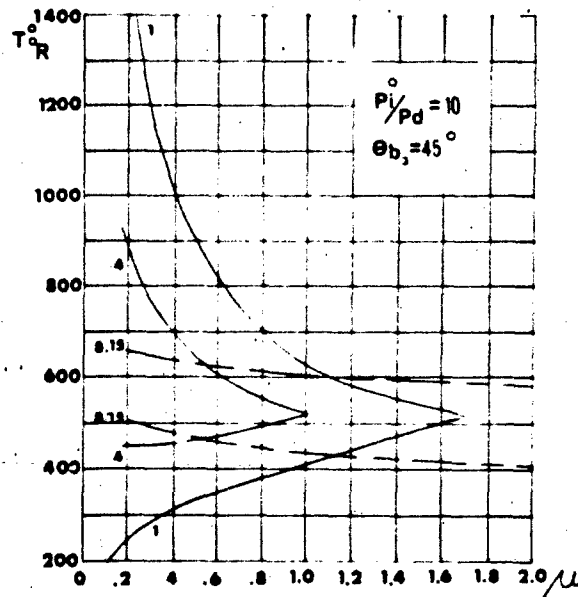
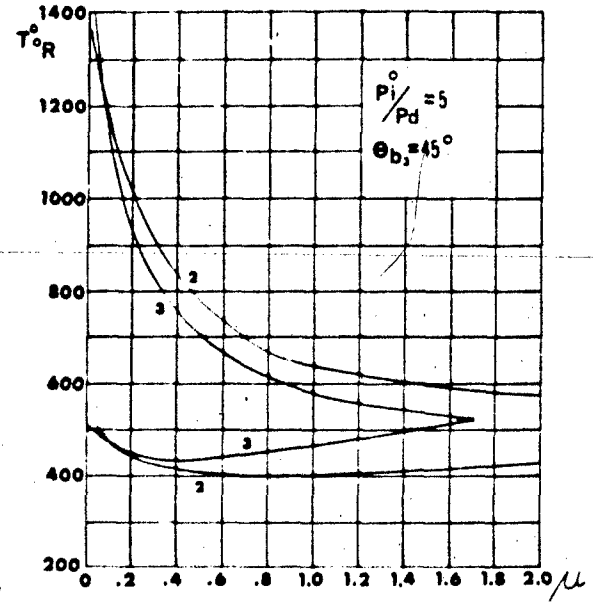
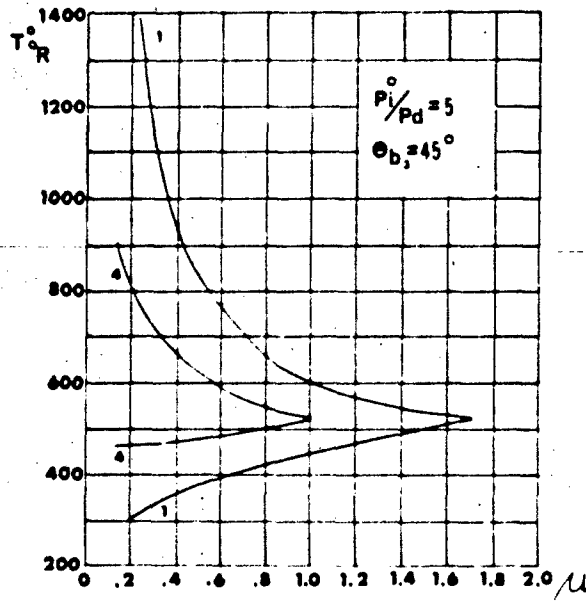


CASE 1 =  $\alpha_{a_1} = 60^{\circ}$   
CASE 4 =  $\alpha_{a_1} = \alpha_{b_1} = \alpha_{a_2} = 90^{\circ}$

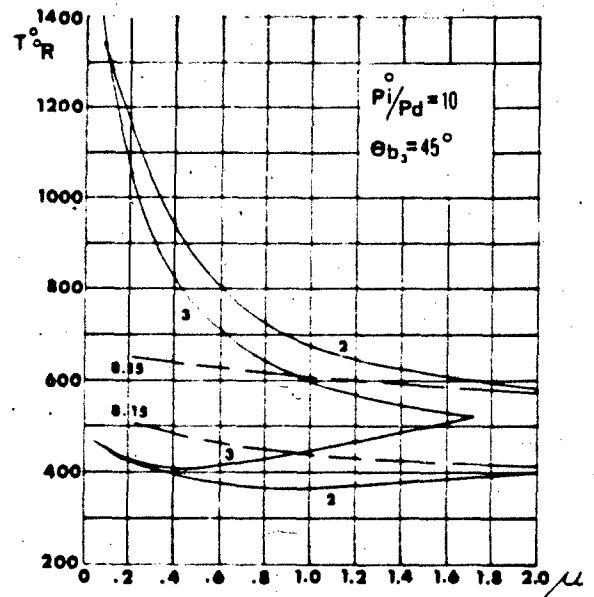


CASE 2 =  $\alpha_{a_1} = \alpha_{b_1} = 60^{\circ}$   
CASE 3 =  $\alpha_{a_1} = 60^{\circ}$

FIG. II-20

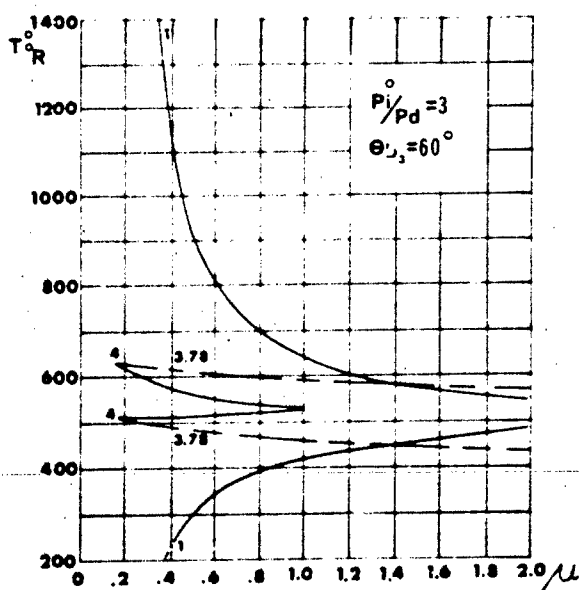
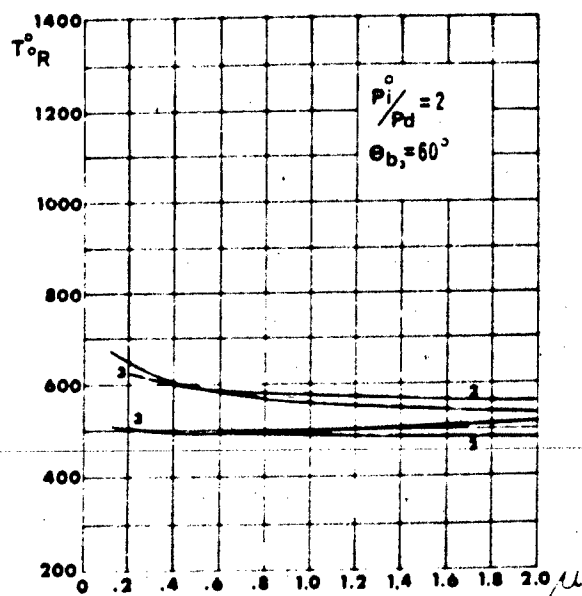
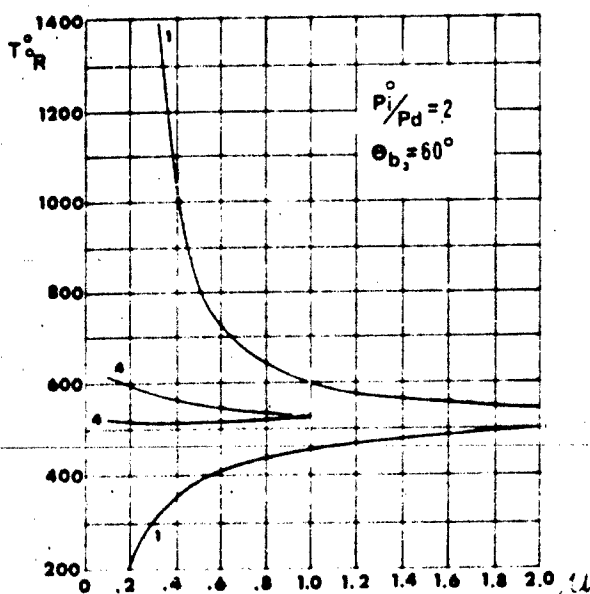


CASE 1 =  $\alpha_{a_1} = 60^{\circ}$   
CASE 4 =  $\alpha_{a_1} = \alpha_{b_1} = 90^{\circ}$

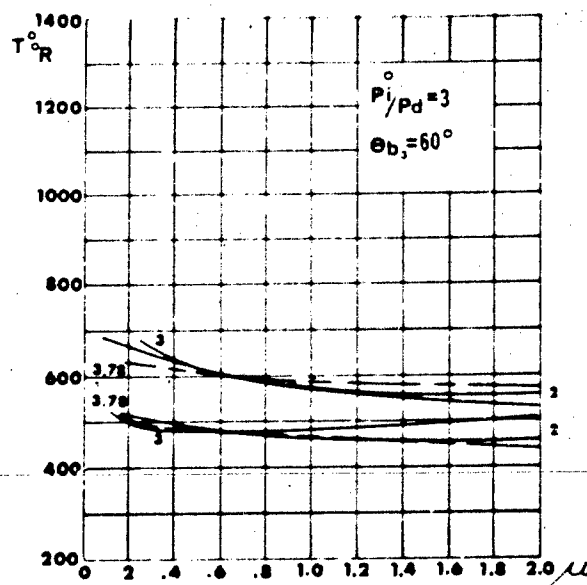


CASE 2 =  $\alpha_{a_1} = \alpha_{b_1} = 60^{\circ}$   
CASE 3 =  $\alpha_{a_1} = 60^{\circ}$

FIG II-21

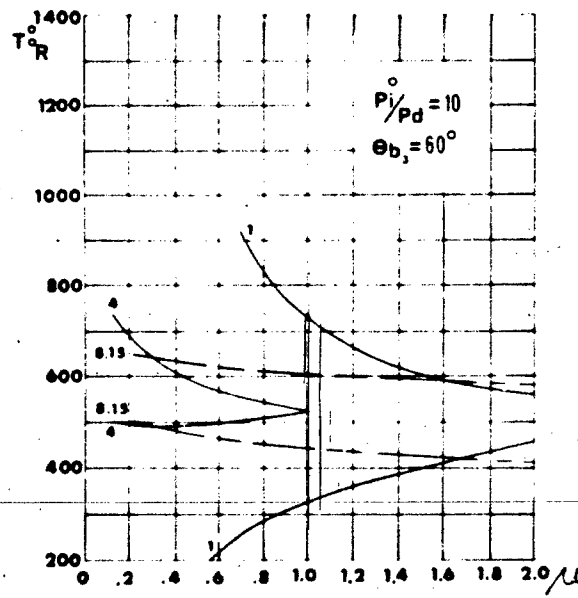
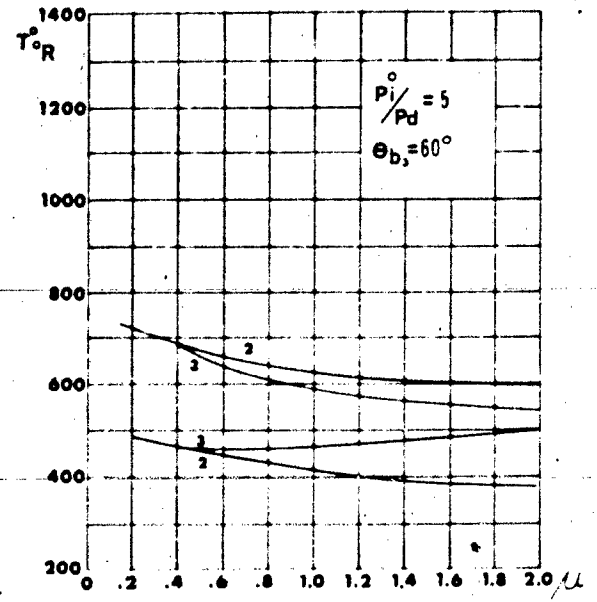
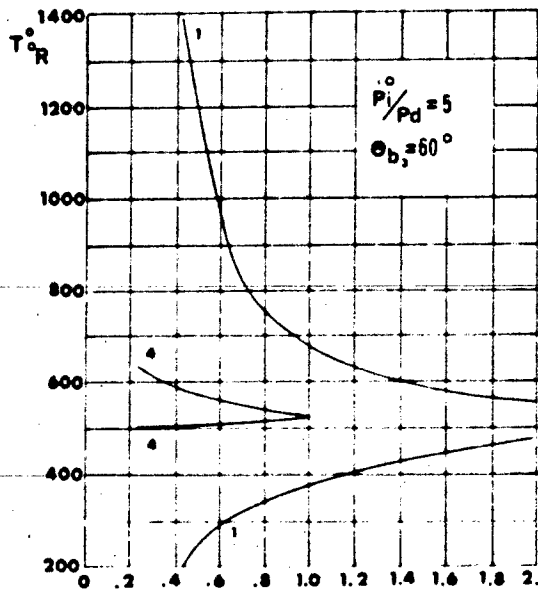


CASE 1 =  $\alpha_a = 30^{\circ}$   
CASE 4 =  $\alpha_a = \alpha_b = \alpha_c = 90^{\circ}$

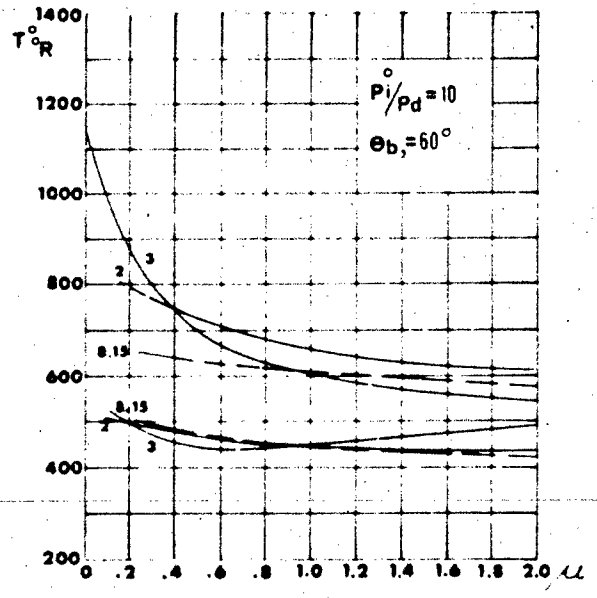


CASE 2 =  $\alpha_a = \alpha_b = 30^{\circ}$   
CASE 3 =  $\alpha_a = 30^{\circ}$

FIG. II-22



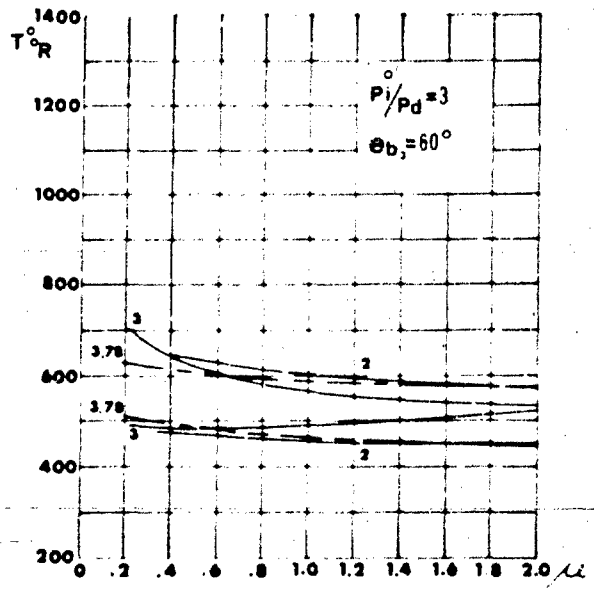
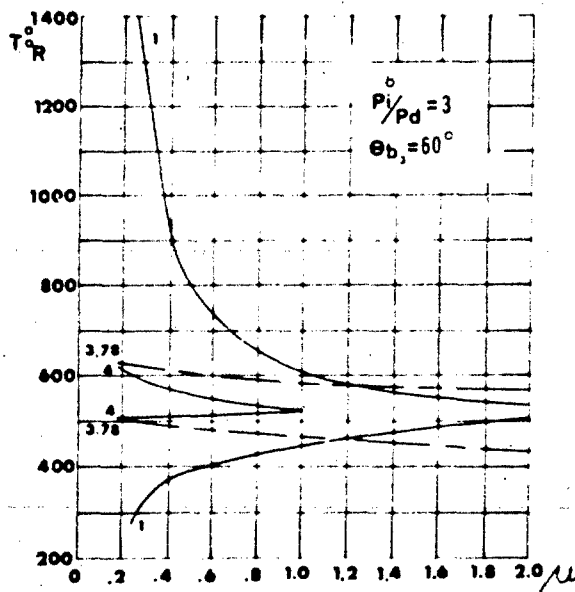
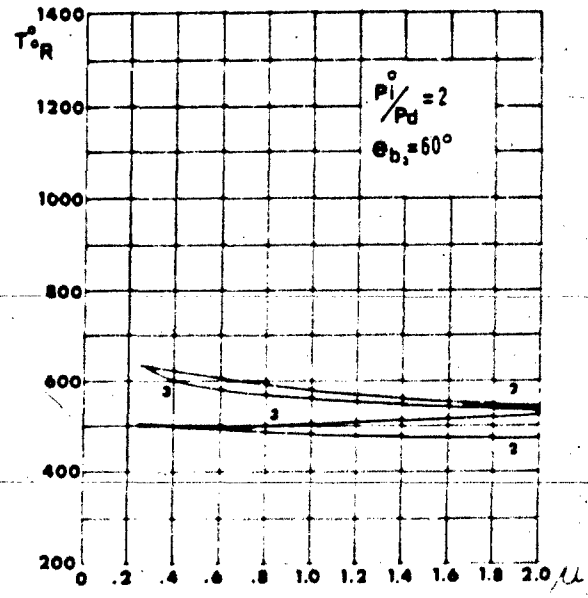
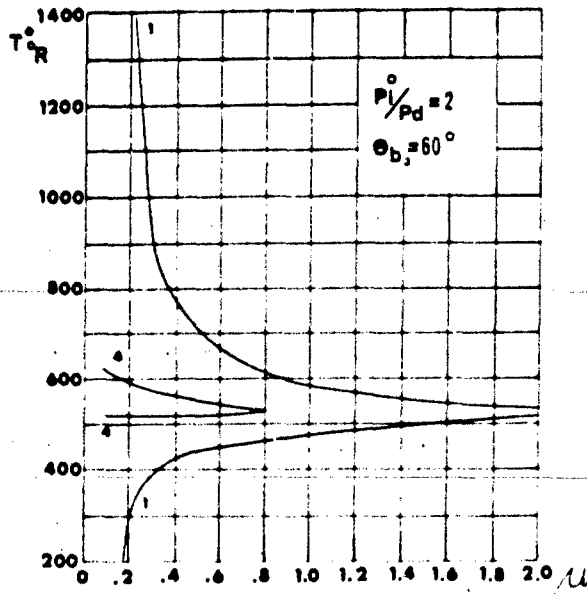
CASE 1 =  $\alpha_{a_1} = 30^{\circ}$   
CASE 4 =  $\alpha_{a_1} = \alpha_{b_1} = \alpha_{a_2} = 90^{\circ}$



CASE 2 =  $\alpha_{a_1} = \alpha_{b_1} = 30^{\circ}$   
CASE 3 =  $\alpha_{a_1} = 30^{\circ}$



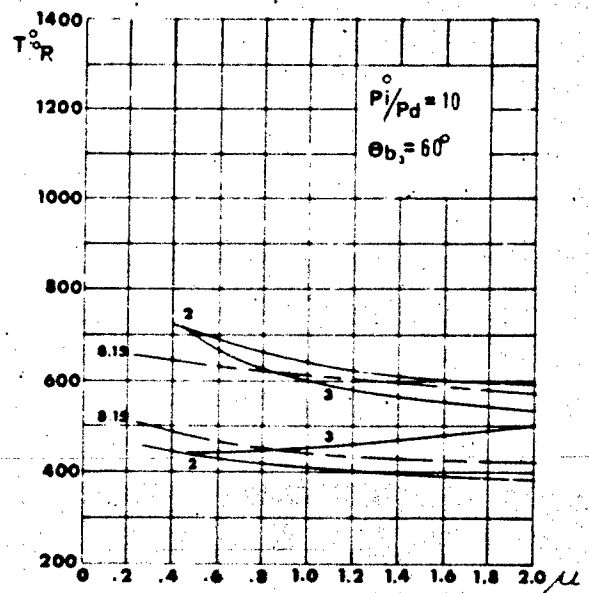
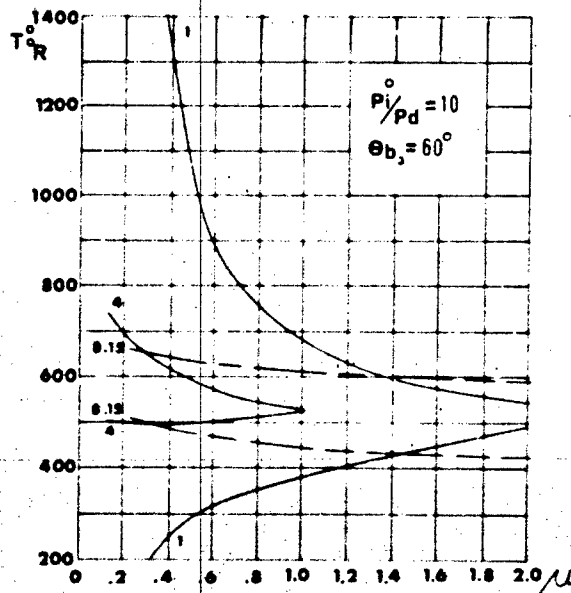
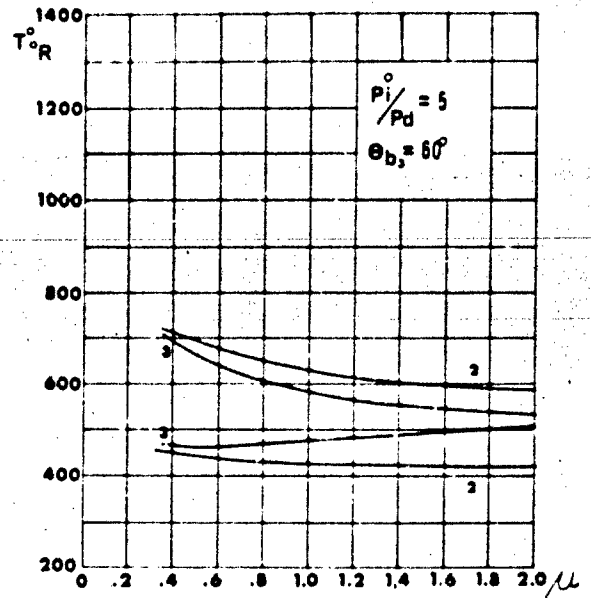
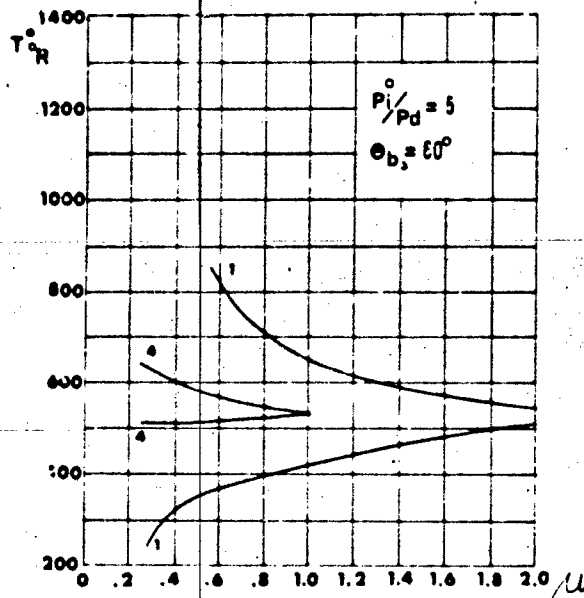
FIG II-23



CASE 1 =  $\alpha_{a_1} = 45^{\circ}$   
CASE 4 =  $\alpha_{a_1} = \alpha_{b_1} = \alpha_{a_2} = 90^{\circ}$

CASE 2 =  $\alpha_{a_1} = \alpha_{b_1} = 45^{\circ}$   
CASE 3 =  $\alpha_{a_1} = 45^{\circ}$

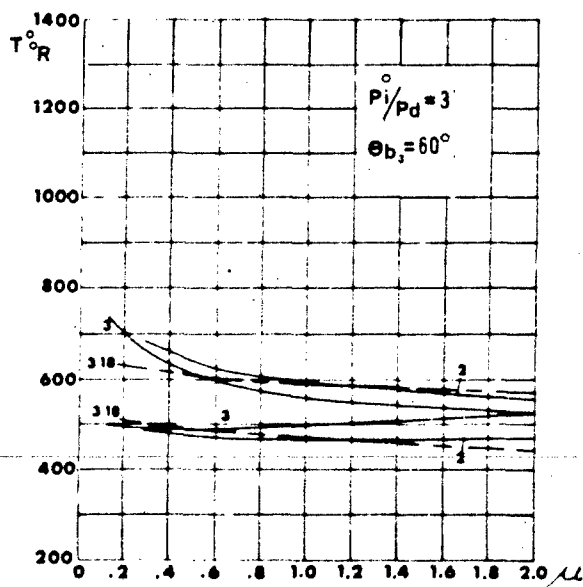
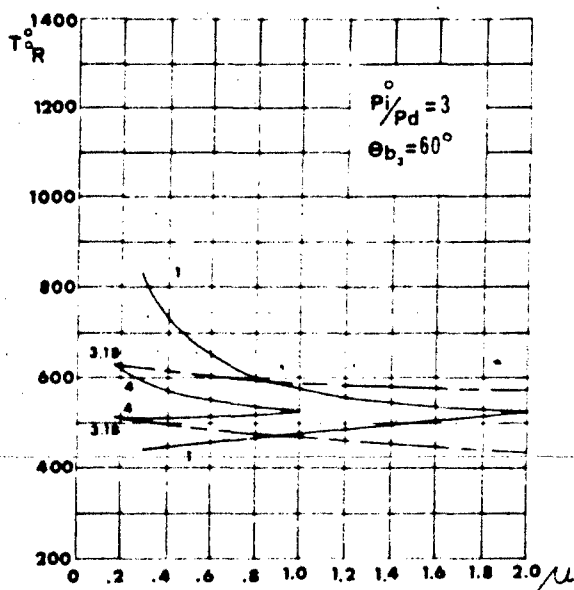
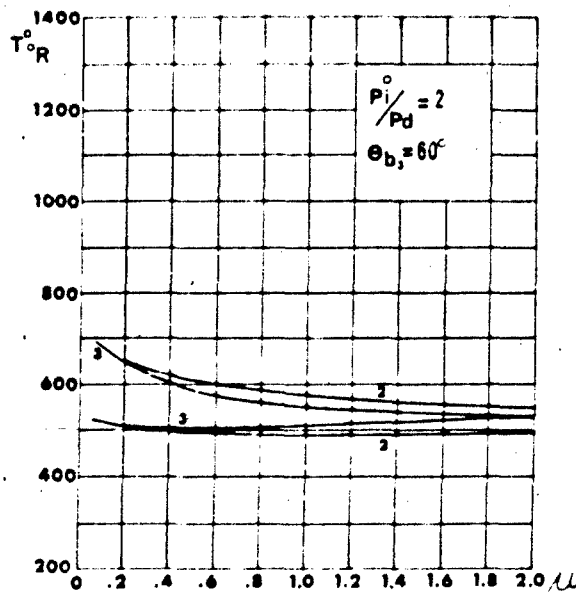
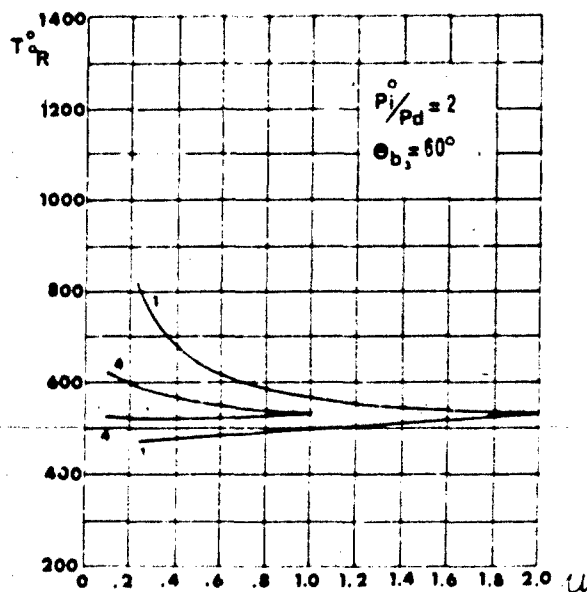
FIG II-24



CASE 1 =  $\alpha_{a1} = 45^{\circ}$   
CASE 4 =  $\alpha_{a1} = \alpha_{b1} = \alpha_{a2} = 90^{\circ}$

CASE 2 =  $\alpha_{a1} = \alpha_{b1} = 45^{\circ}$   
CASE 3 =  $\alpha_{a1} = 45^{\circ}$

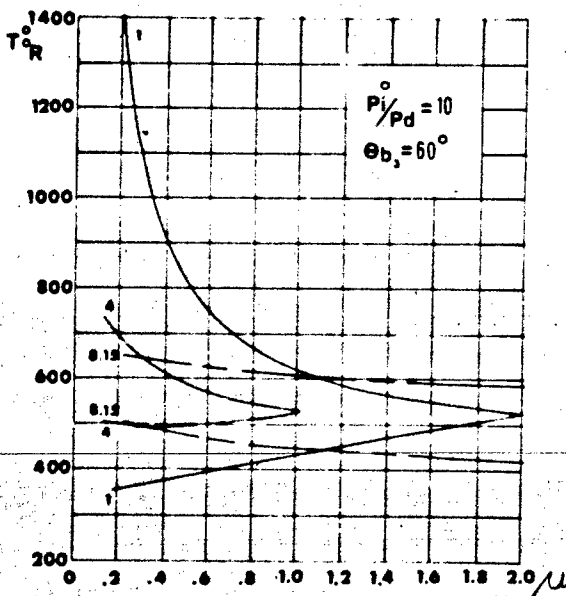
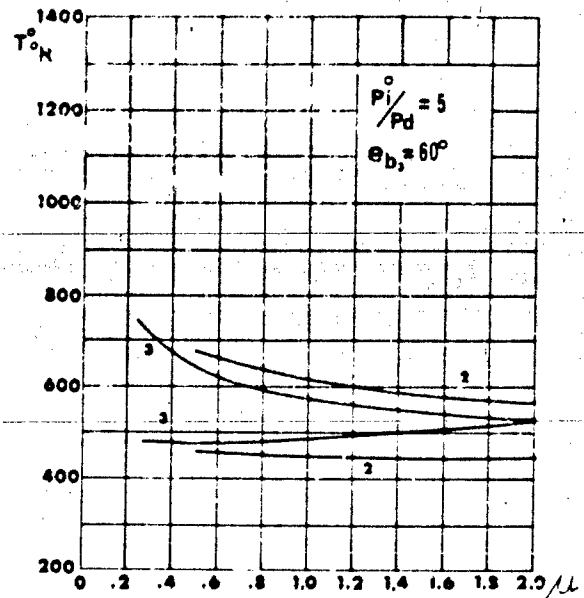
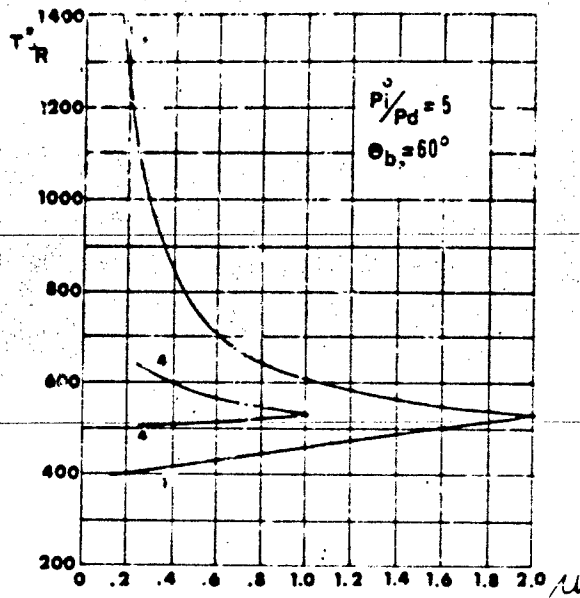
FIG II-25



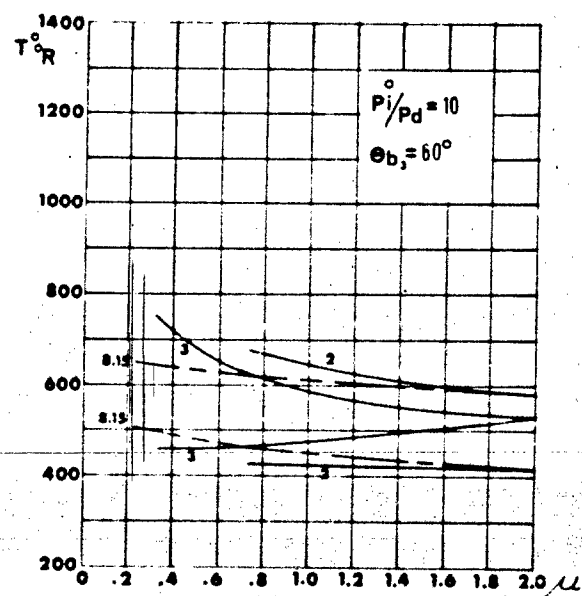
CASE 1 =  $\alpha_{a1} = 60^\circ$   
CASE 4 =  $\alpha_{a1} = \alpha_{b1} = \alpha_{a2} = 90^\circ$

CASE 2 =  $\alpha_{a1} = \alpha_{b1} = 60^\circ$   
CASE 3 =  $\alpha_{a1} = 60^\circ$

FIG II-26



CASE 1 =  $\alpha_{a_1} = 60^{\circ}$   
CASE 4 =  $\alpha_{a_1} = \alpha_{b_1} = \alpha_{a_2} = 90^{\circ}$



CASE 2 =  $\alpha_{a_1} = \alpha_{b_1} = 60^{\circ}$   
CASE 3 =  $\alpha_{a_1} = 60^{\circ}$

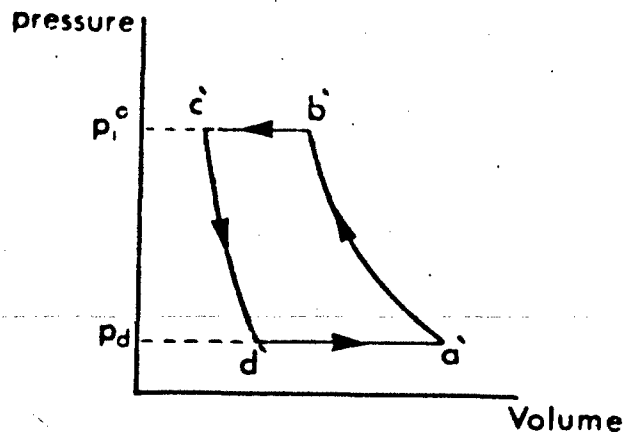


FIG. III-1a STANDARD GAS REFRIGERATION CYCLE

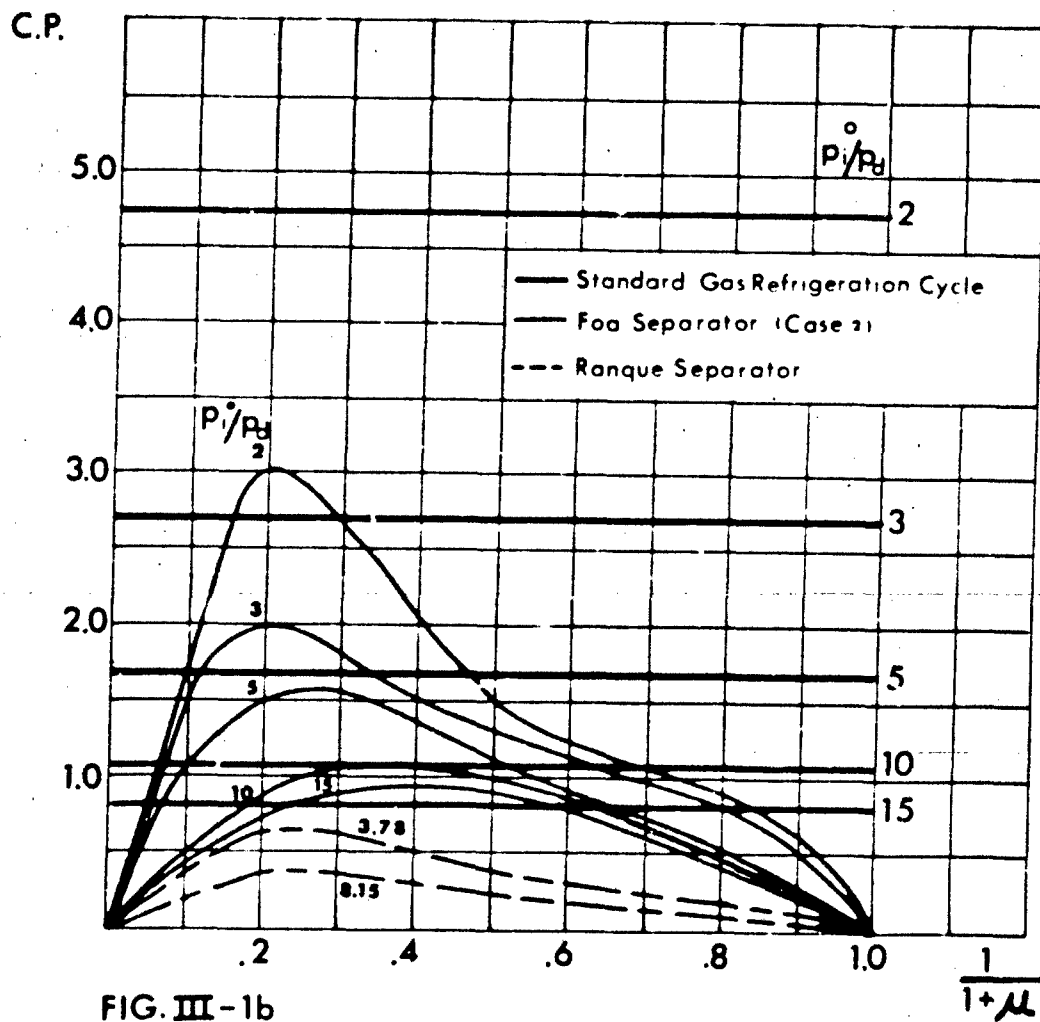


FIG. III-1b

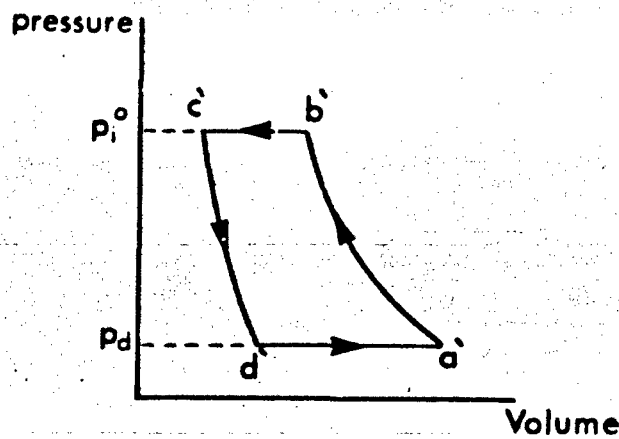


FIG. III-1a STANDARD GAS REFRIGERATION CYCLE

